UNIVERSIDADE D
COIMBRA

João Miguel Nunes Quaresma de Oliveira

Phase diagrams of high-pressure ternary systems

Dissertação no âmbito do Mestrado em Física, ramo de Física da Matéria Condensada, orientada pelo Doutor Tiago Frederico Teixeira Cerqueira e pelo Professor Doutor Fernando Manuel da Silva Nogueira e apresentada ao departamento de Física da Faculdade de Ciências e Tecnologia da Universidade de Coimbra.

Setembro de 2022

Phase diagrams of high-pressure ternary systems

João Miguel Nunes Quaresma de Oliveira

A thesis submitted for the degree of
Master in Physics

FACULDADE DE
CIÊNCIAS E TECNOLOGIA
UNIVERSIDADE D
COIMBRA

Departmente of Physics
University of Coimbra

Advisor
Tiago Frederico Teixeira Cerqueira

Co-Advisor
Fernando Manuel da Silva Nogueira

Coimbra, 23rd September 2022

Phase diagrams of high-pressure ternary systems

Abstract

In recent years, high temperature superconductivity has been reported in several Hydrogen-rich systems under high pressure, being one of the most recent ones a compound in the C-S-H ternary system. The claimed critical temperature was 15 °C at 267 GPa. A common issue in this type of studies is the difficulty in determine the crystal structure of the materials found. Consequently, computational works have proved to be very useful helping these high pressure studies. In this thesis, we searched the H-C-Se, H-Mg-Se and Li-C-S ternary systems for new thermodynamically stable compounds at high-pressure. In order to obtain the lowest energy crystal structures of each $A_xB_yC_z$ compositions, we applied the Minima Hopping Method (MHM) to those ternary systems at a pressure of 150 GPa and at zero temperature, limited by $3 \leq x \leq 7$; $1 \leq y \leq 2$; $1 \leq z \leq 2$ and, if $x \leq 5$, $x + y + z \leq 7$. In total we identified 658 minima, which were selected for further, more accurate, calculations. From these, 5 were found to be thermodynamically stable ($E_{hull} = 0$) with an extra 5 close to stability (under 50 meV/atom), out of which 5 are metallic materials. The 2 thermodynamically stable metallic materials are both from the H-Mg-Se ternary system: $P\bar{3}m1$-Mg_2H_3Se and $Cmm2$-MgH_6Se. The 3 metallic materials close to stability are: $Imm2$-$Mg_2H_3Se_2$, $Immm$-MgH_4Se_2 and $C2/m$-Li_7CS, with a energy distance to the convex hull of 28 meV/atom, 35 meV/atom and 28 meV/atom, respectively. Materials in the H-C-Se ternary system were all found above an energy distance of 100 meV/atom to the convex hull. For the most relevant cases, we also include the correspondent electronic band structures and densities of states.

Diagramas de fase de sistemas ternários a alta pressão

Resumo

Nos últimos anos, tem sido relatada supercondutividade a alta temperatura em vários sistemas ricos em hidrogénio sob alta pressão, sendo um dos mais recentes um composto do sistema ternário C-S-H. A temperatura crítica declarada foi de 15 °C a 267 GPa. Um problema comum neste tipo de estudos é a dificuldade em determinar a estrutura cristalina dos materiais encontrados. Consequentemente, simulações computacionais têm mostrado ser muito úteis para auxiliar esses estudos a alta pressão. Nesta tese, procurámos novos compostos termodinamicamente estáveis nos sistemas ternários H-C-Se, H-Mg-Se e Li-C-S a alta pressão. Para obter as estruturas cristalinas de menor energia de cada estequiometria $A_xB_yC_z$, aplicámos o *Minima Hopping Method* (MHM) a esses sistemas ternários a uma pressão de 150 GPa e a temperatura zero, restringindo-os a $3 \leq x \leq 7$; $1 \leq y \leq 2$; $1 \leq z \leq 2$ e, se $x \leq 5$, $x + y + z \leq 7$. No total, identificámos 658 mínimos, que foram selecionados para cálculos mais precisos. Destes, 5 mostraram-se termodinamicamente estáveis ($E_{hull} = 0$) com mais 5 próximos da estabilidade (abaixo de 50 meV/átomo), dos quais 5 são metálicos. Os 2 materiais metálicos termodinamicamente estáveis são ambos do sistema ternário H-Mg-Se: $P\bar{3}m1$-Mg_2H_3Se e $Cmm2$-MgH_6Se. Os 3 materiais metálicos próximos da estabilidade são: $Imm2$-$Mg_2H_3Se_2$, $Immm$-MgH_4Se_2 e $C2/m$-Li_7CS, com uma distância ao *convex hull* de 28 meV/átomo, 35 meV/átomo e 28 meV/átomo, respectivamente. Materiais no sistema ternário H-C-Se foram todos encontrados acima de uma distância ao *convex hull* de 100 meV/átomo. Para os casos mais relevantes, também incluímos as estruturas de bandas eletrónicas e densidades de estados correspondentes.

Aos meus Pais, Irmão e Irmã.

Contents

List of Abbreviations

T_c Critical Temperature.

BO Born-Oppenheimer.

CASTEP CAmbridge Serial Total Energy Package.

CSP Crystal Structure Prediction.

DAC Diamond Anvil Cell.

DFT Density Functional Theory.

DOS density of states.

EA Evolutionary Algorithms.

FHI-aims Fritz Haber Institute ab initio molecular simulations.

GA Genetic Algorithms.

GGA Generalized Gradient Approximation.

HK Hohenberg-Kohn.

HTSC High Temperature SuperConductivity.

KS Kohn-Sham.

LDA Local Density Approximation.

MD Molecular Dynamics.

MHM Minima Hopping Method.

PAW Projector Augmented Wave.

PBE Perdew–Burke–Erzernhof.

PES Potential Energy Surface.

PSO Particle Swarm Optimization.

QE Quantum ESPRESSO.

USPEX Universal Structure Predictor: Evolutionary Xtallography.

VASP Vienna Ab initio Simulation Package.

VESTA Visualisation for Electronic Structural Analysis.

Chapter 1

Introduction

In recent years, High Temperature SuperConductivity (HTSC) in hydrogen-rich materials has been reported in several systems under high pressure, being one of the most recent ones a compound in the C-S-H ternary system, reaching room temperature superconductivity at 15 °C and 267 GPa [1].

However, given the high pressure apparatuses used, researchers are often unable to determine the crystal structure of these superconductor compounds and, without the crystal structure, a precise evaluation seems impossible. This is one of the many examples where theory and computation play well with experiment: because theorists are not limited by apparatuses, they can help in discovering the structure of these new compounds. This can be done using specialised methods to search for the lowest energy structure of a given composition knowing only the chemical formula, an approach called Crystal Structure Prediction (CSP).

1.1 Motivation

The search for new materials, ultimately in our case, superconductors under extreme pressures, could serve a real life application if any of them turns out to be created at much lower pressure. For example, power lines which would eliminate energy loss due to the resistance of the materials. Obviously, this thought is hypothetical as the search for these high temperature superconductors mainly serves to confirm what Ashcroft pointed: the possibility of having metallic hydrides with high superconducting Critical Temperature (T_c) at a much lower pressure than that of metallic hydrogen [2, 3]. The pressures used both in theoretical and experimental studies are common in the core of celestial bodies thus, this high pressure studies can also be used to better understand those celestial bodies [4]. Consequently, the search for hydrogen-rich compounds

under high pressure has been exhaustive and has led researchers into finding higher and higher T_c superconductors, as we will see further in this section, in Table 1.1.

In 2020, HTSC was claimed in a photochemically synthesized ternary carbonaceous sulfur hydride system (C-S-H) with the superconducting state observed between 140 GPa and 275 GPa in the Diamond Anvil Cell (DAC) and a maximum superconducting T_c of (287.7 ∓ 1.2) K (15°C) achieved at (267 ∓ 10) GPa [1].

Last year, *Gubler et al.* published a work where they could not find theoretical evidence to support the previously stated HTSC. Their extensive structure search, that sampled most of the relevant regions of the C-S-H ternary phase diagram, gave rise to more questions than answers. They doubt that the correct crystal structure was simply overlooked or missed [5]. Furthermore, some publications have questioned the validity of the claimed HTSC [6, 7, 8] and there isn't any experimental reproduction, to our knowledge, to support it. Unsuccessfully, again, to our knowledge, the accurate determination of the possible crystalline structures has proven to be challenging and remains unknown [5].

The high pressure apparatus used to experimentally test the compounds, as already stated, is called a DAC and, very simply, it has two diamonds against each other and the samples are placed in between them, in the smaller side of the diamonds, so that the area is very small to obtain the highest pressure possible. The 150 GPa we are using in our calculations would be very simple to achieve[1] experimentally since conventional DAC can produce pressures of 400 GPa [9] or go to even higher pressures such as 700 GPa [10]. A common image associated to a DAC is simillar to the following:

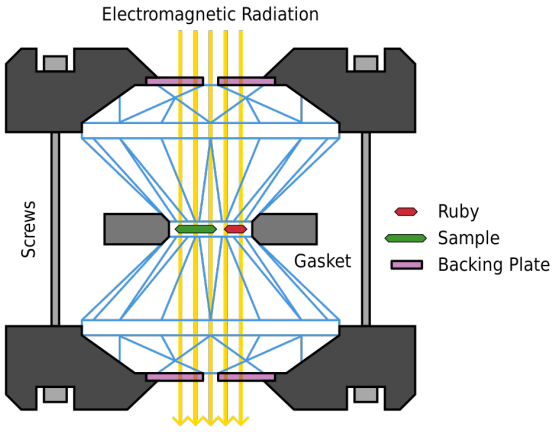

Figure 1.1: Simple cross section of a DAC taken from Wikipedia [11]. We have the structure to tighten the diamonds; in green, the sample in between the diamonds; in red, a ruby that helps measure the pressure since it fluoresces differently with different pressures applied to it; and, in yellow lines, the electromagnetic radiation which can pass through the diamonds and samples and can be used to acquire data.

[1] we are only referring to the pressure side of the experiment

Looking specifically at ternary systems' searches, a big variety of other elements has been added to hydrogen in each of the studies. We shall see a collection of ternary systems at high pressures that have been already explored to some extent in the past few years looking for HTSC. Be aware that some systems might not be present due to being too recent or because they might have escaped our review.

Table 1.1: Ternary hydrides ordered by critical temperature. Compound; space group (spgrp); pressure in GPa; critical temperatures (T_c) in Kelvin; and respective reference. The * indicates a experimental study [1], $(H_2S)(CH_4)H_2$*, that was followed by the theoretical study [5].

Ternary	Compound	Spgrp	Pressure [GPa]	T_c [K]	Ref
Li-F-H	LiF_3H	4	300	0.092	[12]
Li-Au-H	Li_6AuH	71	100	2.79	[13]
Mg-V-H	$MgVH_6$	31	150	27.6	[14]
Fe-Se-H	$FeSeH_6$	6	150	34.4	[15]
La-S-H	$LaSH_6$	63	300	35	[16]
Mg-Sc-H	$MgScH_6$	166	100	41	[17]
Sc-Y-H	$ScYH_6$	200	200	52.907	[18]
Li-Si-H	$LiSi_2H_9$	147	172	54	[19]
Na-Al-H	$NaAlH_8$	123	300	55	[20]
Mg-Si-H	$MgSiH_6$	200	250	63	[21]
Mg-Ge-H	$MgGeH_6$	200	200	67	[22]
Li-Si-H	$LiSiH_8$	12	250	77	[19]
Li-Se-H	$LiSeH_4$	5	200	77	[23]
Ca-B-H	$Ca_2B_2H_{13}$	6	300	89	[24]
Y-Ba-H	$YBaH_8$	123	50; 150	49.6; 89.4	[25]
Y-S-H	YSH_6	131	210	91	[16]
La-B-H	$LaBH_7$	156	110	93	[26]
Ca-S-H	$CaSH_3$	187	128	100	[27]
Li-B-H	Li_2BH_6	225	200	100	[28]
N-Si-H	$NSiH_6$	11	300	110	[29]
Li-Se-H	$LiSeH_6$	25	250	111	[23]
Ca-B-H	$CaBH_6$	205	300	119	[24]
La-B-H	$LaBH_8$	225	55	156	[26, 30]
K-Y-H	KYH_8	12	200; 250; 300	111.3; 122; 163.7	[31]
Li-P-H	$LiPH_6$	200	200	167	[32]
K-Y-H	KYH_{14}	65	300	167.1	[31]
Ca-Y-H	$CaYH_{12}$	221	180	230	[33]
Ca-Y-H	$CaYH_{12}$	65	200	258	[34]
C-S-H	$(H_2S)(CH_4)H_2$*	—	267	287.7	[1]
Mg-Ca-H	$Mg_{0.5}Ca_{0.5}H_6$	229	200	288	[35]
Li-Mg-H	Li_2MgH_{16}	227	250	473	[36]

In Table 1.1, we can see which ternary systems have already been studied and we can use it as an inspiration to choose new ternary combinations. The new combinations are a mixture of a guessing game and an educated guess since all common sense connected to the chemistry side of element combination becomes "distorted" in such extreme pressures. Thus, the new ternary system chosen can simply be based on "a hunch", which comes from a mixture of all available literature and a reminiscent, normal pressure, knowledge which, again, shouldn't be trusted at these high pressures.

The choice of the ternary systems we searched were, given the C-S-H ternary [1, 5], two ternary systems: H-C-Se, trying selenium instead of sulfur, and Li-C-S, having lithium-rich compounds instead of hydrogen-rich. We used Table I of [37] as an inspiration, alongside with Table 1.1, to select the third ternary system, Mg-H-Se.

Examining the studies presented in Table 1.1, they used different types of CSP methods. We can see that most of them used Evolutionary Algorithms (EA) such as Particle Swarm Optimization (PSO) in the Crystal structure AnaLYsis by Particle Swarm Optimization (CALYPSO) package and Genetic Algorithms (GA) in Universal Structure Predictor: Evolutionary Xtallography (USPEX). In [5], we also see the Minima Hopping Method (MHM) being used.

The majority of the Density Functional Theory (DFT) calculations seen in these articles are shared between the Vienna Ab initio Simulation Package (VASP) code [38, 39, 40] and Quantum ESPRESSO (QE) [41, 42] with, fewer times, CAmbridge Serial Total Energy Package (CASTEP) [43] and Fritz Haber Institute ab initio molecular simulations (FHI-aims) software package. We see that ultrasoft pseudopotentials and Troullier–Martin pseudopotentials are widely used. Furthermore, Projector Augmented Wave (PAW) method and Optimized Norm-conserving Vanderbilt pseudopotentials were also used in some of the studies cited. The most used exchange-correlation functional was Perdew–Burke–Erzernhof (PBE) parametrization of the Generalized Gradient Approximation (GGA) with the occasional use of Local Density Approximation (LDA).

Looking at hydrogen-rich systems with lithium and, e.g, as presented in Table 1.1, boron (Li-B-H) [28], fluorine (Li-F-H) [12], magnesium (Li-Mg-H) [36] or phosphorus (Li-P-H) [32], they have the calculated critical temperatures of each compound, in the predicted structures, in a designated pressure between 200 and 300 GPa.

They found $P2_1/m$-LiF_3H ($T_c < 1\,\mathrm{K}$), $Fm\bar{3}m$-Li_2BH_6 ($T_c = 100\,\mathrm{K}$), $Pm\bar{3}$-$LiPH_6$ ($T_c = 200\,\mathrm{K}$) and $Fd\bar{3}m$-Li_2MgH_{16} ($T_c = 473\,\mathrm{K}$). From these theoretical studies, $Fd\bar{3}m$-Li_2MgH_{16} is the most notorious due to the high T_c of an astonishing 473 K at a pressure of 250 GPa.

1.2 Objective

In this thesis, the goal is to use CSP methods to find new materials in the H-C-Se, Mg-H-Se and Li-C-S ternary systems that are stable at high-pressure. Working at a pressure of 150 GPa, we applied the MHM [44, 45, 46] to predict the lowest energy structures in our ternary systems, searching for novel thermodynamic stable compound with signs of having superconducting properties.

These calculations were done using the Vienna Ab initio Simulation Package (VASP code) [38, 39, 40], an implementation of DFT, a successfully established theory [47].

Due to time limitations, we were only able to confirm the thermodynamic stability of the compounds found. We did not have the time to check for dynamical stability through phonon calculations. However, the initial steps of this process were sucessfully completed in this thesis.

1.3 Outline

This thesis is organized in the following way:

Following this introduction, in Chapters 2 and 3, we will present the theoretical background on DFT and MHM, respectively. Then, in Chapter 4, we will clarify structural stability. In Chapter 5 we will present the workflow and our results. Finally, Chapter 6 will have the conclusions and future work.

Chapter 2

Density Functional Theory

The atom is not a simple physical problem and, when we get more and more complexity in our system, things get very complicated, exponentially fast. Going from a hydrogen atom to a helium atom is quite a big jump and getting to a lithium atom is a whole new league. Thankfully, there are ways around this complexity that make the systems calculable in due time. In this chapter we will give the reader some theoretical overview of DFT to see where the complexity arises and how DFT managed to solve some problems. We will use a non-relativistic view, avoiding higher order interactions. To have a cleaner view, we will be using atomic units:

$$\hbar = m_e = e = \frac{1}{4\pi\epsilon_0} = 1 \tag{2.1}$$

2.1 From the Born-Oppenheimer Approximation to DFT

The Born-Oppenheimer (BO) approximation tells us we have electrons in a molecule moving in a field of fixed nuclei [48, 49]. Since the mass difference between electrons and nuclei is really large, the assumption is that we can separate the electronic motion and the nuclear motion in a molecule.

Let us begin with the BO approximation of the non-relativistic time-independent Schrödinger equation, considering a system of N electrons.

$$\hat{H}\Psi(\mathbf{x}_1, \mathbf{x}_2, ..., \mathbf{x}_N) = E\Psi(\mathbf{x}_1, \mathbf{x}_2, ..., \mathbf{x}_N) \tag{2.2}$$

where $\mathbf{x}_i = (\mathbf{r}_i, \sigma_i)$, with $\mathbf{r}_i$ and σ_i being the space and spin coordinates, respectively.

Since the nuclei are fixed, we won't have a kinetic energy term related to the nuclei in our Hamiltonian and the repulsion between nuclei is a constant, E_{nn}. Then, our Hamiltonian will have 3 operators: electron kinetic energy, $\hat{T}$, external potential, $\hat{V}_{ext}$, and electron-electron interaction, $\hat{V}_{ee}$, and the constant E_{nn}[1]. The Hamiltonian can be written as:

$$\hat{H} = \hat{T} + \hat{V}_{ext} + \hat{V}_{ee} + E_{nn} \tag{2.3}$$

each term being:

$$\hat{T} = -\sum_{i=1}^{N} \frac{1}{2}\nabla_i^2, \quad \hat{V}_{ext} = -\sum_{i=1}^{N}\sum_{j=1}^{M} \frac{Z_j}{\mathbf{r}_{ij}}, \quad \hat{V}_{ee} = \sum_{i=1}^{N}\sum_{j>i}^{N} \frac{1}{\mathbf{r}_{ij}} \text{ and } E_{nn} = \sum_{i=1}^{M}\sum_{j>i}^{M} \frac{Z_i Z_j}{\mathbf{r}_{ij}} \tag{2.4}$$

where $\mathbf{r}_{ij} = |r_i - r_j|$, Z_i is the charge of the nuclei i, N is the total number of electrons and M is the total number of nuclei.

The total energy can be written as the sum of a purely electronic energy associated to the 3 operators in our Hamiltonian, E_{elec}, and another value from the constant E_{nn},

$$E = E_{elec} + E_{nn} \tag{2.5}$$

It's a prudent approximation, we have our functions, operators, eigenvalues and nothing appears to discourage our train of thought to obtain the information we want to known about a particular state of our target system. Let's take, e.g., methane, CH_4, which has 10 electrons, consequently 30 coordinates. Having a grid with 10 points would result in 10^{30} entries. Very quickly we see that the solution to a given, apparently "simple", problem is intractable and, furthermore, many of the systems we want to study contain many more atoms and electrons [49]. Just storing the wave-function is a problem on its own and, in addition, the particles are not independent as one can see from the $\hat{V}_{ee}$ operator. DFT became the answer to replace the N-electron wave-function with the 3N spatial variables dependency by the electron density, $n(\mathbf{r})$, a simpler quantity depending on 3 spatial variables that is an observable and can be measured experimentally [49] and, with an auxiliary system, reduce as much as possible the approximations needed to solve the systems.

This electron density, $n(\mathbf{r})$, that gives the probability of finding one of the N electrons within the volume $d\mathbf{r}_i$, is defined as [49]:

$$n(\mathbf{r}) = N \int |\Psi(\mathbf{r}, \sigma_1, \mathbf{x}_2, \mathbf{x}_3, ..., \mathbf{x}_N)|^2 d\sigma_1 d\mathbf{x}_2 d\mathbf{x}_3 ... d\mathbf{x}_N \tag{2.6}$$

[1]The operator eigenfunctions are unaffected by the addition of a constant, conversely the same operator eigenvalues will be affected by having that constant value added to them.

Highlighting that the integrals are over all spatial coordinates but one, $d\mathbf{r}$ and, clearly, the integration of $n(\mathbf{r})$ over $d\mathbf{r}$ gives the number of electrons, N.

Given that electrons are indistinguishable, the probability of finding a given electron in the volume element $d\mathbf{r}$ is the same for each one of the other electrons so we have the N electrons multiplication in Equation 2.6.

2.2 The Hohenberg-Kohn Theorems

Now we will see both Hohenberg-Kohn (HK) theorems in the case of non-degenerate ground states[2]. The "**Proof of Existence**" states that V_{ext} is a unique functional of $n(\mathbf{r})$ up to a constant [49, 50]. The maps [51, 52]:

$$\hat{V}_{ext} \rightarrow \Psi \rightarrow n \tag{2.7}$$

are clearly defined and surjective. But are they also injective, i.e., can we define $n \rightarrow \Psi \rightarrow \hat{V}_{ext}$?

Based on *reductio ad absurdum*, we begin by considering 2 Hamiltonians, similar to the Hamiltonian in Equation 2.3, that differ only in the external potential, V_{ext} and V'_{ext},

$$\hat{H} = \hat{T} + \hat{V}_{ee} + \hat{V}_{ext} \tag{2.8}$$
$$\hat{H}' = \hat{T} + \hat{V}_{ee} + \hat{V}'_{ext} \tag{2.9}$$

For the first arrow in 2.7 we presume that the external potentials, V_{ext} and V'_{ext}, are distinguished by more that a constant and lead up to the same ground state wave-function, Ψ_0. Applying the Hamiltonians to Ψ_0,

$$\hat{H}|\Psi_0\rangle = (\hat{T} + \hat{V}_{ee} + \hat{V}_{ext})|\Psi_0\rangle = E_0|\Psi_0\rangle \tag{2.10}$$
$$\hat{H}'|\Psi_0\rangle = (\hat{T} + \hat{V}_{ee} + \hat{V}'_{ext})|\Psi_0\rangle = E'_0|\Psi_0\rangle \tag{2.11}$$

Subtracting both equations,

$$(\hat{V}_{ext} - \hat{V}'_{ext})|\Psi_0\rangle = (E_0 - E'_0)|\Psi_0\rangle \tag{2.12}$$

Evidently, the external potentials, V_{ext} and V'_{ext}, are only different by a constant and so, with this condition, the external potential determines the ground state wave-functions.

[2]The presented reasoning depends on the fact that the ground state energy is the lowest possible energy of the system.

Secondly, to map $n \rightarrow \Psi$, we will have 2 different ground state wave-functions, Ψ_0 and Ψ_0', coming from the same electron density, $n(\mathbf{r})$. The ground state wave-functions, Ψ_0 and Ψ_0', and ground state energies, E_0 and E_0', are associated to $\hat{H}$ and $\hat{H}'$, respectively [49, 53]. Applying the variational principle,

$$\begin{aligned} \langle \Psi_0' | \hat{H}' | \Psi_0' \rangle &< \langle \Psi_0 | \hat{H}' | \Psi_0 \rangle & (2.13) \\ E_0' &< \langle \Psi_0 | \hat{H}' + \hat{H} - \hat{H} | \Psi_0 \rangle & (2.14) \\ E_0' &< \langle \Psi_0 | \hat{H} | \Psi_0 \rangle + \langle \Psi_0 | \hat{H}' - \hat{H} | \Psi_0 \rangle & (2.15) \end{aligned}$$

Since $\hat{V}_{ext}$ and $\hat{V}_{ext}'$ are the only difference between both Hamiltonians,

$$E_0' < E_0 + \langle \Psi_0 | \hat{V}_{ext}' - \hat{V}_{ext} | \Psi_0 \rangle \tag{2.16}$$

Switching between primed and unprimed quantities, the same calculations are applied,

$$\begin{aligned} \langle \Psi_0 | \hat{H} | \Psi_0 \rangle &< \langle \Psi_0' | \hat{H} | \Psi_0' \rangle & (2.17) \\ E_0 &< E_0' + \langle \Psi_0 | \hat{V}_{ext} - \hat{V}_{ext}' | \Psi_0 \rangle & (2.18) \end{aligned}$$

Because we have 2 different ground state wave-functions, Ψ_0 and Ψ_0', producing the same electron density, $n(\mathbf{r})$:

$$E_0' < E_0 + \langle \Psi_0 | \hat{V}_{ext}' - \hat{V}_{ext} | \Psi_0 \rangle => E_0' < E_0 + \int n(\mathbf{r}) [\hat{v}_{ext}' - \hat{v}_{ext}] d\mathbf{r} \tag{2.19}$$

$$E_0 < E_0' + \langle \Psi_0 | \hat{V}_{ext} - \hat{V}_{ext}' | \Psi_0 \rangle => E_0 < E_0' - \int n(\mathbf{r}) [\hat{v}_{ext}' - \hat{v}_{ext}] d\mathbf{r} \tag{2.20}$$

Finally, the addition of both Equations 2.19 and 2.20 gives:

$$E_0' + E_0 < E_0 + E_0' \tag{2.21}$$

This absurd conclusion reveals that different ground state wave-functions do not produce the same electron density. This fulfils the maps in 2.7 and we assure a one-to-one correspondence between the external potential and the electronic density. The maps 2.7 are in, in fact, injective. Since we can obtain the wave-function from the density and the wave-function contains the information about the system, every observable can be written as a functional of the density [51].

Let's take Equation 2.3 and write the energy as a functional of the density [50, 53]:

$$E_v[n] = \langle\Psi|(\hat{T}+\hat{V}_{ext}+\hat{V}_{ee}+E_{nn})|\Psi\rangle \tag{2.22}$$

$$E_v[n] = \langle\Psi|(\hat{T}+\hat{V}_{ee})|\Psi\rangle + \int n(\mathbf{r})v_{ext}d\mathbf{r} + E_{nn} \tag{2.23}$$

$$E_v[n] = F_{HK}[n] + \int n(\mathbf{r})v_{ext}d\mathbf{r} + E_{nn} \tag{2.24}$$

The HK functional,

$$F_{HK}[n] = T[n] + E_{ee}[n] \tag{2.25}$$

is the sum of both the electrons' kinetic energy and the electron-electron interaction energy [49]. This functional, $F_{HK}[n]$, is a universal functional and for a given number of particles is the same for any external potential.

The HK functional, $F_{HK}[n]$, is utopian since, unfortunately, there is no known form and it needs to be approximated. If it were known, it would solve Schrödinger's equation exactly [49].

The second theorem, "**Variational Principle**", responsible for DFT be labeled a "ground state only theory" [49], states that for any non-negative trial density $\tilde{n}(\mathbf{r})$ that satisfies $\int \tilde{n}\mathbf{r}d\mathbf{r} = N$, associated with some external potential $\tilde{v}_{ext}$, will result in the ground state energy if, and only if, the input density is the true ground state density [47, 49, 53]. Then we have $E_0 \leq E_{\tilde{v}_{ext}}[\tilde{n}]$.

If we minimize $E_v[n]$, employing the variational principle,

$$E_0 = \min_{\{n\}} E_v[n] \tag{2.26}$$

adding a Lagrange multiplier, μ, the chemical potential, to fix N, the number of particles in the system, we can also write,

$$\frac{\delta}{\delta n(\mathbf{r})}\left(E_v[n] - \mu\left(\int n(\mathbf{r})d\mathbf{r} - N\right)\right) = 0 \tag{2.27}$$

$$\frac{\delta}{\delta n(\mathbf{r})}\left(F_{HK}[n] + \int n(\mathbf{r})v_{ext}d\mathbf{r} + E_{nn} - \mu\left(\int n(\mathbf{r})d\mathbf{r} - N\right)\right) = 0 \tag{2.28}$$

Leading to the following Euler-Lagrange equation,

$$\frac{\delta F_{HK}}{\delta n(\mathbf{r})} + v_{ext} - \mu = 0 \tag{2.29}$$

By solving 2.29 we would obtain the ground state electron density. Again, if we knew the exact $F_{HK}[n]$, this would also be an exact equation. Having an approximation we can still apply this method to any system.

2.3 Kohn-Sham Scheme

We still have all the electrons interacting through the $\hat{V}_{ee}$ operator so let's change the problem [54]. W. Kohn and L.J. Sham changed it from a many body problem to an independent particle problem [55]. They created a new auxiliary system which assumes that the original system and the new independent particle system, the auxiliary system, have the same ground state density.

Because we are dealing with independent fermions, and non-degenerate ground states, the exact wave-function is a Slater determinant of one-electron wave-funtions, ϕ_i [49].

Futhermore, our auxiliary system will have the following Hamiltonian,

$$\hat{H}_{aux} = \hat{T}_{aux} + \hat{V}_{aux} \tag{2.30}$$

Where $\hat{T}_{aux}$ is the independent particle kinetic energy operator and $\hat{V}_{aux}$ is an effective potential operator, in the auxiliary system. The following Schrödinger equation is satisfied:

$$\left[-\frac{\nabla^2}{2} + v_{aux}(\mathbf{r})\right]\phi_i(\mathbf{r}) = \epsilon_i\phi_i(\mathbf{r}) \tag{2.31}$$

and the ground state electron density is calculated with the N lowest occupied orbitals [51], given by,

$$n(\mathbf{r}) = \sum_{i=1}^{occ} |\phi_i(\mathbf{r})|^2 \tag{2.32}$$

The energy in the auxiliary system is;

$$E_{v_{aux}}[n] = T_{aux}[n] + \int n(\mathbf{r})v_{aux}(\mathbf{r})d\mathbf{r} \tag{2.33}$$

If we apply an analogous procedure used in Equation 2.27, the functional derivative will be:

$$\frac{\delta}{\delta n(\mathbf{r})}\left(T_{aux}[n] + \int n(\mathbf{r})v_{aux}d\mathbf{r} - \mu_{aux}\left(\int n(\mathbf{r})d\mathbf{r} - N\right)\right) = 0 \tag{2.34}$$

yielding the Euler-Lagrange equation,

$$\frac{\delta T_{aux}[n]}{\delta n(\mathbf{r})} + v_{aux} - \mu_{aux} = 0 \tag{2.35}$$

Since both systems were assumed to have the same ground state electron density the solution

to Equations 2.29 and 2.35 are identical. We can rewrite F_{HK} as

$$F_{HK}[n] = T_{aux}[n] + E_H[n] + E_{xc}[n] \tag{2.36}$$

Where $E_H[n]$ is the Hartree energy, a classical electrostatic energy,

$$E_H[n] = \frac{1}{2}\int \frac{n(\mathbf{r})n(\mathbf{r}')}{|\mathbf{r}-\mathbf{r}'|}d\mathbf{r}d\mathbf{r}' \tag{2.37}$$

and the exchange-correlation energy, E_{xc},

$$E_{xc}[n] = (T[n] - T_{aux}[n]) + (E_{ee}[n] - E_H[n]) = \Delta T[n] + E_{ncl}[n] \tag{2.38}$$

where, because $T_{aux}[n] \neq T[n]$, $\Delta T[n]$ is the residual part of the true kinetic energy added to the non-classical electrostatic contributions, $E_{ncl}[n]$, [49]. The exchange and correlation energy is small enough to make this approximation extremely reliable, nevertheless, this term plays a part in the quantum mechanical complications we do not know exactly how to handle so we just "swept them under the rug" [47, 52].

By substituting the newly modified functional 2.36 in Equation 2.28 we get:

$$\frac{\delta}{\delta n(\mathbf{r})}\left(T_{aux}[n] + E_H[n] + E_{xc}[n] + \int n(\mathbf{r})v_{ext}d\mathbf{r} + E_{nn} - \mu\left(\int n(\mathbf{r})d\mathbf{r} - N\right)\right) = 0 \tag{2.39}$$

resulting in:

$$\frac{\delta T_{aux}}{\delta n(\mathbf{r})} + v_H[n] + v_{xc}[n] + v_{ext} - \mu = 0 \tag{2.40}$$

with,

$$v_H[n] = \int \frac{n(\mathbf{r})}{|\mathbf{r}-\mathbf{r}'|}d\mathbf{r}' \text{ and } v_{xc}[n] = \frac{\delta E_{xc}[n]}{\delta n(\mathbf{r})} \tag{2.41}$$

Following this last equation, switching the functional derivative of T_{aux} in Equation 2.35, we get:

$$v_{aux} = v_H[n] + v_{xc}[n] + v_{ext} - \mu + \mu_{aux} \tag{2.42}$$

HK proof of existence theorem allows v_{ext} to add μ and μ_{aux} to itself and give the same electron

density and, reordering the terms, we shall change v_{aux} to its most common name, Kohn-Sham (KS) potential, v_{KS}, written as:

$$v_{KS}[n](\mathbf{r}) = v_{ext}(\mathbf{r}) + v_H[n] + v_{xc}[n] \tag{2.43}$$

and we can rewrite Equation 2.40:

$$\frac{\delta T_{aux}}{\delta n(\mathbf{r})} + v_{KS}[n](\mathbf{r}) - \mu = 0 \tag{2.44}$$

We see that Equations 2.44 and 2.35 are analogous and the ground state electron density can be obtained through the one-electron Schrödinger equation:

$$\left[-\frac{\nabla^2}{2} + v_{KS}[n](\mathbf{r})\right]\phi_i(\mathbf{r}) = \epsilon_i\phi_i(\mathbf{r}) \tag{2.45}$$

and the ground state electron density is obtained exactly like Equation 2.32,

$$n(\mathbf{r}) = \sum_{i=1}^{occ} |\phi_i(\mathbf{r})|^2 \tag{2.46}$$

These last 2 equations are called the KS equations [51]. The total energy is then given by,

$$E_{KS}[n] = T_{aux}[n] + \int n(\mathbf{r})v_{ext}d\mathbf{r} + \frac{1}{2}\int \frac{n(\mathbf{r})n(\mathbf{r}')}{|\mathbf{r}-\mathbf{r}'|}d\mathbf{r}d\mathbf{r}' + E_{xc}[n] + E_{nn} \tag{2.47}$$

The approximation needed for F_{HK} is reduced to the approximation of E_{xc} [51]. One may say that we are repeating ourselves, and we are, after all, if we knew the exact forms of the exchange-correlation the solution would be also be exact.

Chapter 3

Crystal structure Prediction

CSP was, without a doubt, an important development made in the beginning of this century. To portray the difficulty of this method, in 1994, almost thirty years ago, "No" was the answer to the question "Are Crystal Structures Predictable?"[56]. Thought to be impossible, CSP was achieved due to advancements in *ab initio* codes, unveiling new materials before any experimental evidence or analysis.

In simple terms, CSP means finding the stable crystal structure knowing only the chemical formula. The number of possible minima grows exponentially with the number of atoms and, given that the systems tend to be extremely complex, a exhaustive search might be impracticable. We clearly see that this is no simple task. However, due to the fact that these algorithms are essentially heuristic, they can find a reasonable solution in a reasonable time. As one might imagine, the longer we search, the higher the probability of finding the global minimum of a given system. In spite of that, there is no way for us to clearly identify the global minimum, but practice showed that solutions are often close to the solution. One of the objectives made possible by CSP was, and still is, finding HTSC has we saw in Table 1.1 from Chapter 1.1.

The CSP method we will be focusing on is the MHM, developed by S. Goedecker and M. Amsler [45, 46], but other CSP methods exit, such as: basin-hopping, random search, Simulated Annealing, Metadynamics, EA [44]. As of today, the most used are the EA, mainly, GA and PSO. Despite the differences between EA and the MHM, on average, they yield equivalent results [57].

3.1 Minima Hopping Method

The MHM, as we already stated, is a CSP algorithm used to search for the lowest energy structure knowing only the chemical formula. With the objective of efficiently searching the Potential Energy Surface (PES) of our system, the MHM algorithm jumps between the basin[1], with an implementation to avoid revisiting already explored regions and avoid the worst search directions. This is coupled with short Molecular Dynamics (MD) runs followed by a geometry optimization of the landing site structure, to obtain a local minimum, with the overall objective of finding the global minimum [46]. There is an energy interval that is continuously being updated in such a way that, on average, half of the moves are accepted/rejected. Evidently, we could revisit an already explored space or be confined in high energy barriers. This is avoided with a continuous regulation of the temperature of the MD runs. During the search, the temperature value is not only increased if one falls back into the current minimum, but also if we get into another minimum that had already been visited. The more times we revisit an already identified minimum, the higher the temperature gets to allow the algorithm to escape to unexplored space and, with more new minina, the temperature will gradually decrease, allowing a more thorough work [46].

An idea taken from the Bell–Evans–Polanyi principle is also applied to haste the minimization [58]. The analogy is based on the lowest activation energy, i.e, the lowest barrier that a reaction overcomes will fall in the lowest energy product. If we switch the reaction by a minimum going over a potential energy barrier, there is a high probability of crossing the lowest energy barrier and obtain a lower minimum [46].

This procedure is called “softening” and applies a bias to the initial velocities of the MD simulation for the escape step. However, to avoid becoming a deterministic process by preferably pointing towards a low energy barrier, it’s mainly used to eliminate components of the velocity on hard modes, i.e., in the high energy barriers directions [45].

The MHM has been used in a variety of different systems, in specific, in high-pressure systems [5, 59], such as the work we are presenting.

[1] The zone that, using simple small-step relaxation on the lower energy direction, contains all the configurations that will relax into a minimum of the PES.

Chapter 4

Structural Stability

After finding a new compound, we want to study it experimentally, which means that we first need to be able to actually make it in the laboratory. The first step is to know the compound's formation energy and all the possible decomposition channels.

For example, in a given A-B binary system, we have the compound A_xB_y with energy $E_{A_xB_y}$. This compound's formation energy, which is the difference between the compound's energy and the sum of the energies of the elementary phases, is $E_{form} = E_{A_xB_y} - [xE_A + yE_B]$. If $E_{form} > 0$, the compound is not stable. However, if $E_{form} < 0$, we only know that the compound is stable against the decomposition to elementary phases. There might be another composition with a lower formation energy and we need to know if there is a decomposition channel that leads to this lower energy compound. The compounds could, e.g., decompose into $A_xB_{y-1} + B$ and we wouldn't be able to know it until we computed $E_{form} = E_{A_xB_y} - \left[E_{A_xB_{y-1}} + E_B\right]$

The calculation of multiple formation energies of stable and metastable compounds for all possible decomposition channels, allows us to create the *convex hull* of thermodynamic stability. This hull is a hypersurface in composition space, which contains the thermodynamically stable compounds [60]. The energy distance to the convex hull is defined as the difference between the formation energy and the surface of the convex hull. Consequently, if the energy distance to the convex hull is zero, the compound is thermodynamically stable; if the energy distance to the convex hull is small (we considered small to be under 50 meV/atom[1]), the compound is metastable [61, 62, 63]; and it is thermodynamically unstable for higher energy distances.

To have a visual aid, we have a convex hull example from the hypothetical A-B binary system in Figure 4.1 where α_1, α_2, β_1 and β_2 are four different crystalline structures with chemical composition A_xB_y for some x and y. We can see in Figure 4.1 that the solid line is the convex

[1]The motivation to label compounds below 50 meV/atom as metastable will be clarified in Chapter 5.

hull and α_1 and β_1 are both on the convex hull, i.e, they are thermodynamically stable phases. Meanwhile, α_2 and β_2 are both above the hull, which means they are not stable.

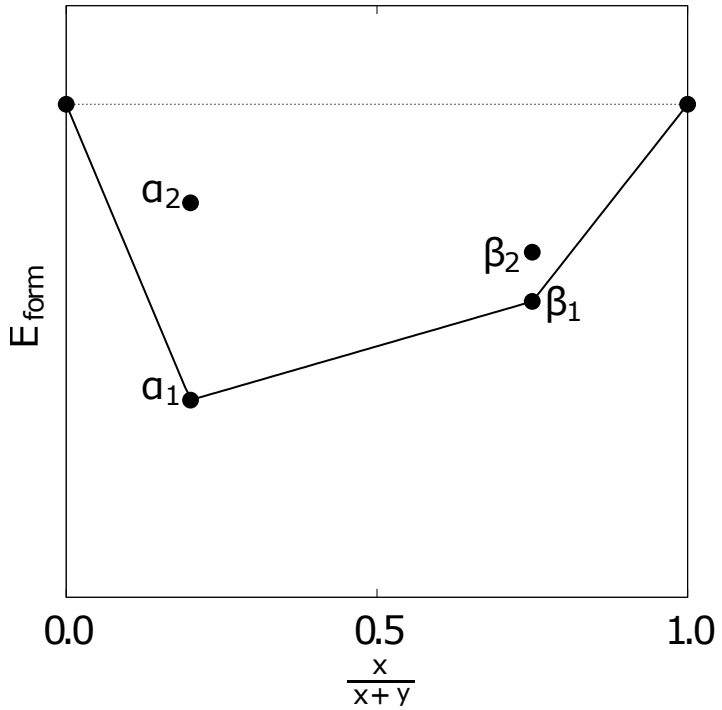

Figure 4.1: Example of the convex hull of the hypothetical A-B binary system, with the possible A_xB_y compositions, with 2 compounds on the convex hull, α_1 and β_1, and 2 compounds above the convex hull, α_2 and β_2. [64]

In principle, we would need to know all the possible decomposition channels to build the convex hull. As this is not possible, we rely on all the known experimentally or theoretically thermodynamically stable compounds. Through the use of DFT, we calculate them all in the same conditions used in the simulations that delivered the compound we want to test for thermodynamic stability.

In this thesis, instead of using the formation energy, we use the formation enthalpy because we are doing our calculations under pressure, 150 GPa to be exact. Remembering thermodynamics, enthalpy is:

$$H = U + PV \tag{4.1}$$

where U is the internal energy from the interactions and positions of the constituents of the system, P is the pressure surrounding the system, and V is the volume of the system. If there is some change in the system, the result will be the initial enthalpy plus its variation, ΔH. Maintaining the same pressure, P, and having a possible variation in the internal energy, ΔU, and in the volume, ΔV, we will have

$$H + \Delta H = U + \Delta U + P(V + \Delta V) = H + \Delta U + P\Delta V \tag{4.2}$$

Clearly, $\Delta H = \Delta U + P\Delta V$ and so we have an enthalpy variation because the internal energy changed, the volume changed, or both [65].

However, the thermodynamic stability is not the only requirement to have a high confidence that our compound is experimentally attainable. The compound might be thermodynamically stable but dynamically unstable, i.e., the geometrical arrangement of the atoms might not be the lowest energy one. We investigate this through the calculation of the phonon spectrum, where, if no imaginary phonon frequencies are found, we have dynamic stability. If we find imaginary frequencies, the state we are considering is not the ground state. The imaginary frequencies show that our thermodynamically stable structure is, in fact, in a saddle-point, i.e, we are in a local minimum in one direction but there is another direction where the potential energy decreases.

In short, if we have thermodynamic stability and dynamic stability, i.e., the distance to the convex hull is zero and we do not have imaginary frequencies in the phonon spectrum, our compound is stable within the precision of our theory. Beyond this, the material might not be experimentally accessible due to, e.g, the existence of other competing phases or lack of a synthesis pathway of the material itself.

Chapter 5

Workflow and results

In this chapter we will guide the reader through the method used to go from the first randomly generated structures to the final thermodinamically stable structures. We will follow with the results of our search.

5.1 Workflow

We applied the MHM to the ternary systems H-C-Se, H-Mg-Se[1] and Li-C-S at a pressure of 150 GPa and at zero temperature. For each system, from all the possible $A_xB_yC_z$ compositions, we restrict ourselves to those with $3 \leq x \leq 7$; $1 \leq y \leq 2$; $1 \leq z \leq 2$ and, if $x \leq 5$, $x + y + z \leq 7$.

As the starting point for the MHM runs, for each stoichiometry, we generated random initial geometries limited by inter-atomic distances greater or equal to the sum of the covalent radii. The initial random cell is created so the MHM has a starting structure to begin the runs and the limitation is to eliminate any covalent radii overlap. We did this twice for both one and two formula unit cells to have different starting points for the MHM runs. The MHM searches were performed using the PBE [66] approximation to the exchange-correlation functional using default "high" accuracy energy cutoffs.

To have a better converged structure, we performed a higher accuracy geometry optimization maintaining a pressure of 150 GPa and at zero temperature within DFT in the PAW formalism [67] as implemented in the VASP code[2] [38, 39, 40]. The energy cutoff was set to 520 eV along with the precision set to high. The k-point grids were chosen to ensure that convergence would be better than 2 meV per atom. If the density of k-point per atom obtained was less that the

[1] H-Mg-Se and Mg-H-Se are the same ternary system.
[2] VASP 5.4.4

reference used in the Materials Project calculations [68], we would use the Materials project one.

The flowchart of Figure 5.1 summarizes the method for a given composition in a ternary system.

Let us describe the workflow in 3 sections. First, the MHM ran its search until we obtained at least 30 minima. Then, we would stop the search and, for each of the lowest energy, select 12 different structures in each composition and a new geometry optimization with stricter criteria would be performed. Finally, a summary of the results would yield not only the enthalpy per atom but also some other relevant values such as band gap value and space group.

Secondly, in order to evaluate the thermodynamic stability of the newly discovered compounds, we needed information on the convex hull at 150 GPa. Unfortunately, this information was not available in one centralized database and required a thorough review of the available theoretical or experimental literature related to high-pressure structure studies. Furthermore, some of the work we found didn't have the crystal structures available or the needed information to fully reconstruct the crystal structures. This literature review lead to Tables 5.1 and 5.2, where we summarize the structures used to build the convex hull. For compatibility, we re-optimized these structures at 150 GPa using the same parameters we use for our calculations. We then built the convex hull using the PYMATGEN library [69]. As one might see, the convex hull didn't take all the structures from Tables 5.1 and 5.2. That's why we numbered the compounds in those tables, to specify which structures were used in each phase diagram. By definition, the compounds are thermodynamically stable if the energy distance to the convex hull is zero. Within a distance of 50 meV we will consider the compound metastable.

The 50 meV/atom mark is motivated by: the containment of errors associated with the approximations used in the calculated values [61]; a clear manifestation that materials within 40 to 50 meV/atom of the convex hull are synthesizable [61, 62, 63, 70]; and, mainly, to be overly cautious since there are different studies calling "metastable" to materials above 100 meV/atom without a clear justification.

Finally, we calculated the density of states (DOS) and electronic band structure of some of the metallic compounds. We present three DOS and band structures for each ternary system followed by a snapshot of the crystal structure (created using the Visualisation for Electronic Structural Analysis (VESTA) software [71]).

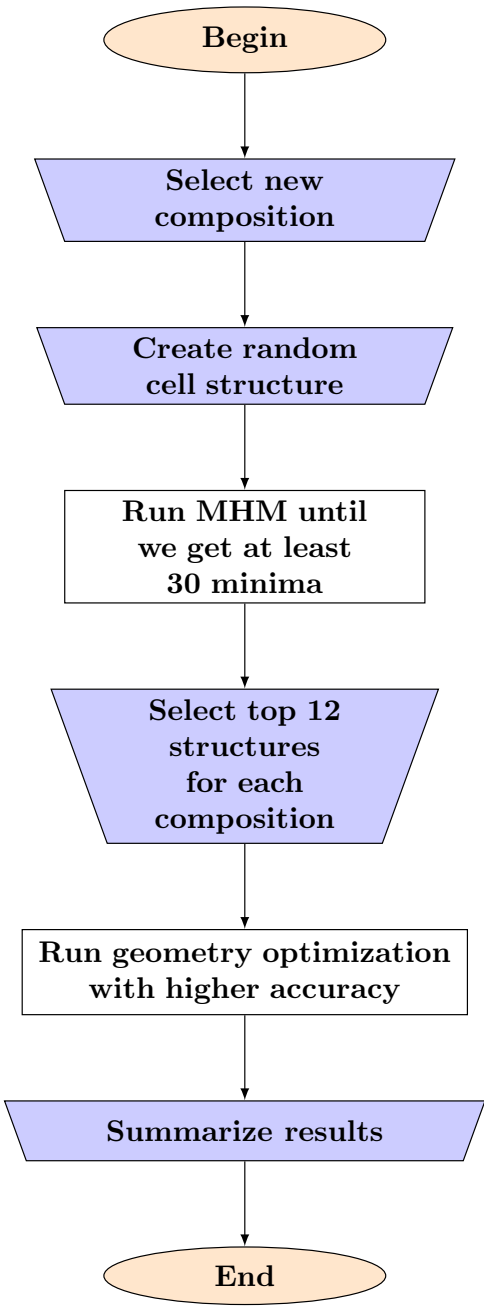

Figure 5.1: Flowchart to obtain all structures with different compositions for each of the ternary systems.

Table 5.1: First part of convex hull data: number for reference (#); compound; number of atoms in the structure (N_{atoms}); pressure of the compound, and space group taken from the respective reference (spgrp); space group taken from our calculations with VASP (spgrp-V); and respective references. The compounds are all from theoretical studies.

#	Compound	N_{atoms}	Pressure [GPa]	Spgrp	Spgrp-V	Ref
1	H	12	250	—	64	[5]
2	H	4	100	194	194	[72]
3	H	8	100	29	29	[72]
4	H	8	100	14	14	[72]
5	H	16	100	176	176	[72]
6	H	24	300	15	15	[72]
7	H	48	300	15	15	[72]
8	H	48	300	60	60	[72]
9	H	24	300	5	5	[72]
10	H	16	300	72	72	[72]
11	H	8	300	64	64	[72]
12	H	24	300	64	64	[72]
13	H	8	500	64	69	[72]
14	Li	20	70	41	41	[73]
15	Li	28	220	64	64	[73]
16	Li	12	70	5	5	[73]
17	Li	24	80	61	64	[73]
18	Li	12	100	64	64	[73]
19	Li	12	100	41	64	[73]
20	Li	16	350	135	135	[73]
21	Li	2	450	166	166	[73]
22	Li	2	450	74	74	[73]
23	Li	2	500	227	277	[73]
24	Mg	2	0	229	229	[68] MP-110
25	Se	2	0	229	229	[68] MP-119
26	S	8	250	—	166	[5]
27	C	2	250	—	227	[5]

Table 5.2: Second part of convex hull data: number for reference (#); compound; number of atoms in the structure (N_{atoms}); pressure of the compound, and space group taken from the respective reference (spgrp); space group taken from our calculations with VASP (spgrp-V); some notes (if nothing is said, the compound is theoretical; if the compound was experimentally synthetized (exp); if the compound is metastable (meta). Compounds number 29 and 31 were not run since we have compounds 28 and 30 closer to 150 GPa); and respective references.

#	Compound	N_{atoms}	Pressure [GPa]	Spgrp	Spgrp-V	Notes	Ref
28	HSe_2	12	200	12	12		[74]
29	HSe_2	12	300	12		not run	[74]
30	H_3Se	8	200	229	229		[74]
31	H_3Se	8	300	229		not run	[74]
32	HSe	4	300	129	129		[74]
33	H_2Se	9	0	152	42		[74]
34	HSe_2	12	300	15	15	meta	[74]
35	H_2Se	12	300	12	12	meta	[74]
36	H_3Se	16	50	12	74	meta	[74]
37	H_3Se	8	300	2	12	meta	[74]
38	HSe	32	300	14	14	meta	[74]
39	HSe_2	6	300	53	53	meta	[74]
40	H_3Se	12	200	166	229	meta	[74]
41	MgH_4	20	100	63	63		[75]
42	MgH_{16}	34	130	2	2		[75]
43	MgH_2	6	180	194	194		[75]
44	ζ-MgH_2	6	180	194	194		[75]
45	ϵ-MgH_2	12	10	62	62		[75]
46	MgH_{12}	39	140	148	148		[75]
47	CH_3	32	250	—	14		[5]
48	CH_4	20	250	—	1		[5]
49	CH_2	12	250	—	63		[5]
50	CH_6	7	250	—	8		[5]
51	CH_2	12	100	63	63		[76]
52	CH_3	16	100	14	14		[76]
53	LiC_2	12	40	63	63		[77]
54	Li_2C_2	8	19.3	71	71	exp	[77]
55	Li_2C_2	8	40	71	71		[77]
56	Li_2C_2	16	19.3	62	62	exp	[77]
57	Li_2C_2	16	35	62	62		[77]
58	Li_2S	6	18.8	62	194		[78]
59	C_2S_4	6	250	—	2		[5]
60	C_4S_4	8	250	—	2		[5]

5.2 Results

In this section, we will discuss in detail the results obtained with the MHM runs. The number of structures found in the MHM runs were 658 and, after further calculations, we obtained 10 below 50 meV/atom, out of which 5 are metallic, as can be seen in Table 5.3

Table 5.3: The compound; number of atom in the structure (N_{atoms}); energy distance to the convex hull below 50 meV/atom (E_{hull}); space group (spgrp); and Band gap in eV.

Compound	N_{atoms}	E_{hull} [meV/atom]	Spgrp	Band gap [eV]
Mg_2H_3Se	6	0	164	0.0
MgH_6Se	8	0	35	0.0
Mg_2H_6Se	9	0	38	1.2
MgH_4Se	12	0	8	1.7
MgH_7Se	18	17	8	1.0
$Mg_2H_3Se_2$	7	28	44	0.0
MgH_4Se_2	14	36	71	0.0
MgH_5Se	14	46	8	0.2
Li_6CS	16	0	141	2.6
Li_7CS	18	28	12	0.0

5.2.1 Li-C-S ternaty system

For the Li-C-S ternary system, the number of structures found in the MHM runs were 230. The compounds from Tables 5.1 and 5.2 used to define the convex hull were the numbers 18, 26, 27, 57 and 58.

As we can see in Table 5.4, Li_6CS is on the convex hull, which means that it is thermodynamically stable. Li_7CS is metastable at 28 meV/atom from the convex hull. The other compounds are between 100 to 500 meV/atom above the convex hull, therefore they are less likely to be able to be synthesized. The phase diagram can be viewed in Figure 5.2.

We calculated the electronic band structure and DOS for the following compounds: $C2/m$-Li_7CS, 28 meV/atom above hull; $R3m$-Li_7C_2S 94 meV/atom above hull; and $P\bar{1}$-Li_6C_2S 129 meV/atom above hull, which were the three closest ones to the convex hull of Table 5.4.

The electronic bands structures and DOS in Figures 5.9, 5.8 and 5.10 confirm these are metals.

We also present the crystal structures of each of these compounds in Figure 5.6, made with the aid of the VESTA software with a description of the respective crystal structure.

Table 5.4: Convex hull data of the Li-C-S ternary system, at 150 GPa, ordered from the lowest to the highest energy distance from the convex hull. The compound; number of atom in the structure (N_{atoms}); energy distance to the convex hull in meV/atom (E_{hull}); space group (spgrp) and Band gap in eV. The compounds from tables 5.1 and 5.2 used to make the convex hull were the numbers 18, 26, 27, 57 and 58.

Compound	N_{atoms}	E_{hull} [meV/atom]	spgrp	Band gap [eV]
Li_6CS	16	0	141	2.6
Li_7CS	18	28	12	0.0
Li_7C_2S	10	94	160	0.0
Li_6C_2S	18	129	2	0.0
Li_5CS	14	140	10	0.5
$Li_7C_2S_2$	11	141	12	0.0
Li_7CS_2	20	141	12	0.0
Li_6CS_2	9	219	156	0.6
Li_4C_2S	14	251	2	0.0
Li_4CS	12	256	59	0.0
Li_3CS	10	355	8	0.0
Li_3C_2S	6	424	1	0.0
Li_3CS_2	12	435	6	0.0
Li_4CS_2	14	455	6	0.0
$Li_3C_2S_2$	7	483	12	0.0

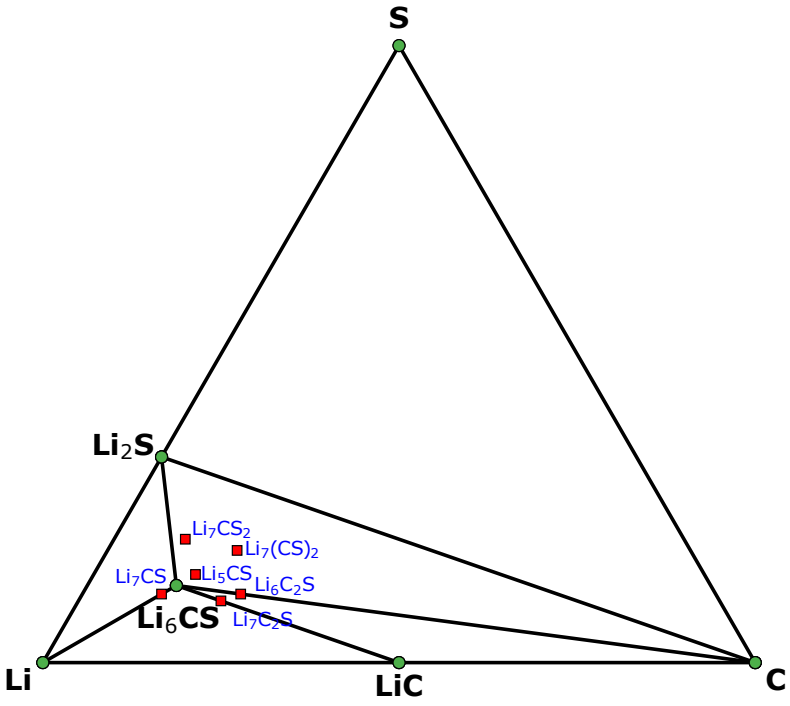

Figure 5.2: Phase diagram of the Li-C-S ternary system at 150 GPa. In green we have the thermodynamically stable compounds and, in red, the compounds above the convex hull.

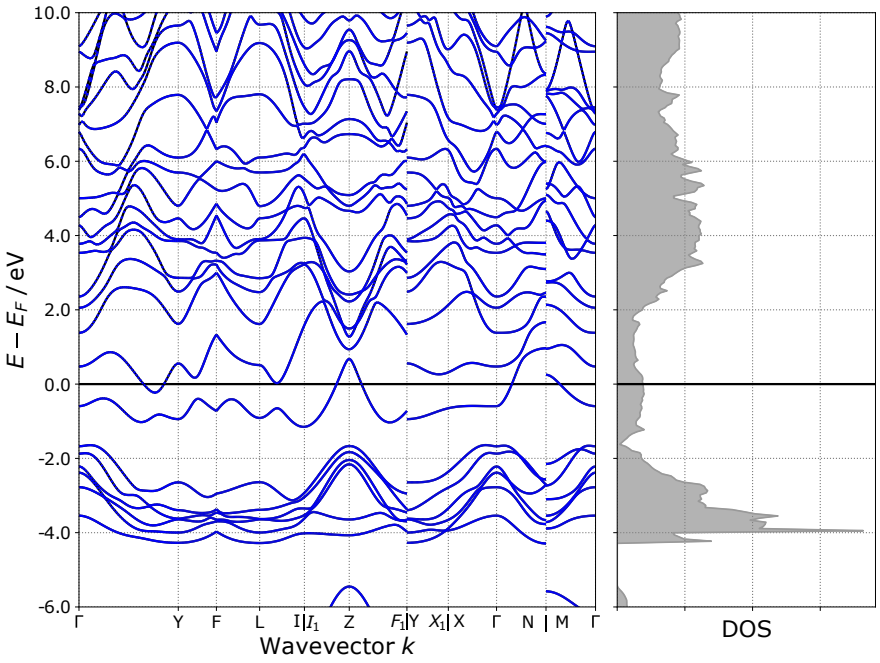

Figure 5.3: Electronic band structure and DOS of $C2/m$-Li_7CS with an energy above the convex hull equal to 28 meV/atom. In the vertical axis, we set the Fermi energy at zero. In the horizontal axis, in the electronic band structure we have the high symmetry points; on the right we have the total density of states.

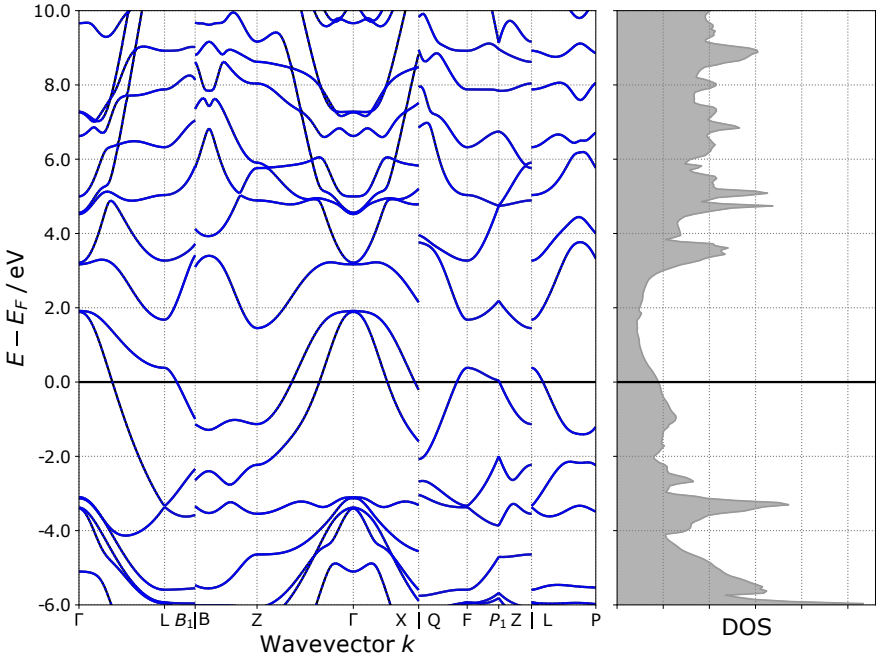

Figure 5.4: Electronic band structure of $R3m$-Li_7C_2S with an energy above the convex hull equal to 94 meV/atom. In the vertical axis, we set the Fermi energy at zero. In the horizontal axis, in the electronic band structure we have the high symmetry points; on the right we have the total density of states.

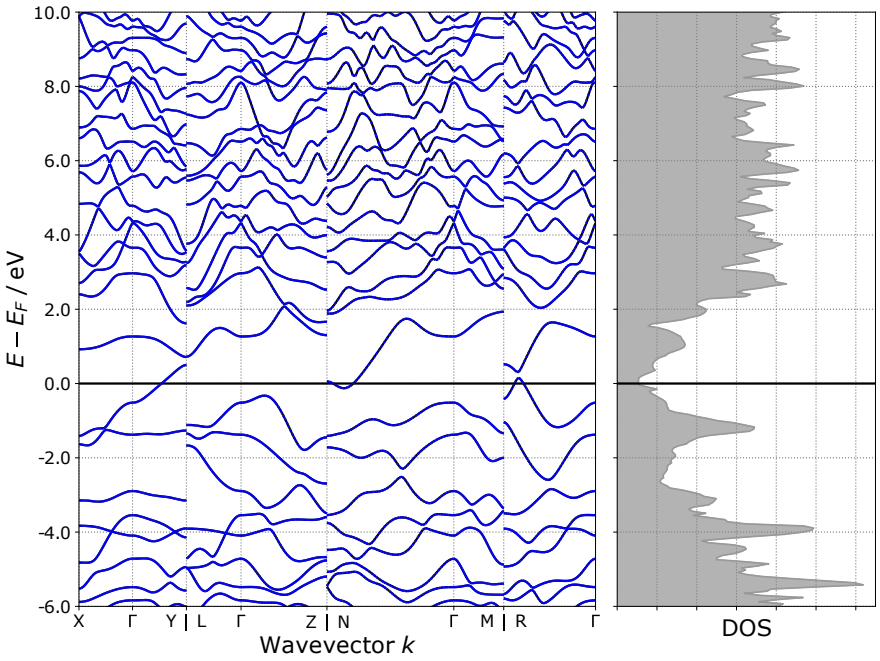

Figure 5.5: Electronic band structure of $P\bar{1}$-Li_6C_2S with an energy above the convex hull equal to 129 meV/atom. In the vertical axis, we set the Fermi energy at zero. In the horizontal axis, in the electronic band structure we have the high symmetry points; on the right we have the total density of states.

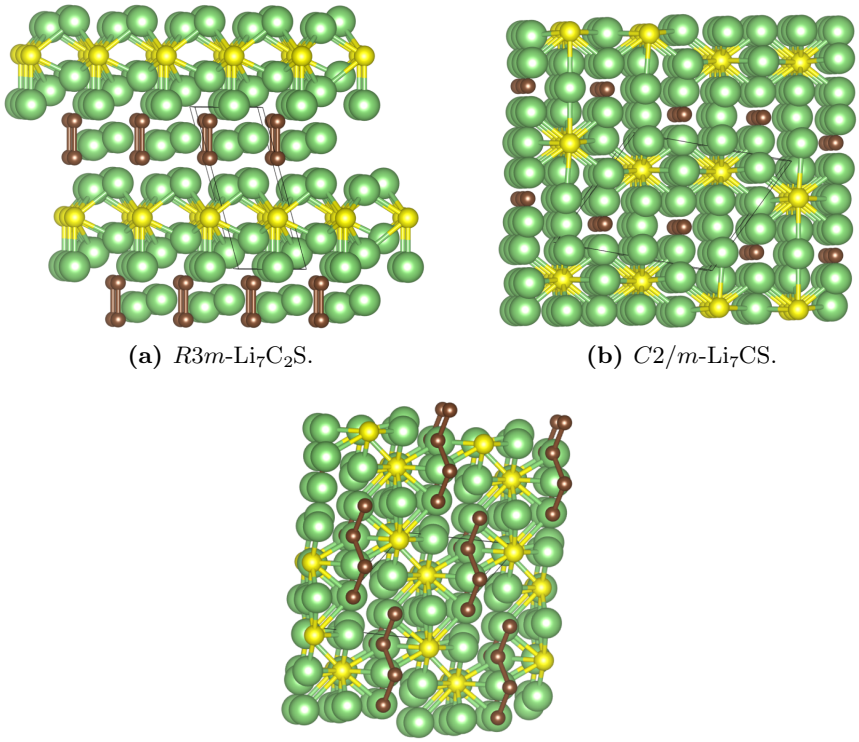

(a) $R3m$-Li_7C_2S. **(b)** $C2/m$-Li_7CS.

(c) $P\bar{1}$-Li_6C_2S.

Figure 5.6: Crystal structure of the compounds from the band structures presented from the Li-C-S ternary system. We have lithium (Li) in green, carbon (C) in brown and sulfur (S) in yellow.

- Li_7C_2S in Figure 5.6(a) has two "layers": one made of C and Li atoms and another made of S atom in between Li atoms (more Li atoms in the bottom part). Another point of view can reveal a honeycomb shape made of Li atoms with Li, C or S in the center of the hexagonal shape, depending on the layer we are watching.
- Li_7CS in Figure 5.6(b) has straight lines of C or S atom in between the Li atoms. Also, from other two different directions, we can see a honeycomb structure, with Li, C or S in the center of the hexagonal shapes, and a grid like structure.
- Li_6C_2S in Figure 5.6(c) has groups of four C atoms in a small zigzag, entangle in between the Li-S structure. This Li-S structure has S atoms almost fully surrounded by the Li atoms.

5.2.2 H-C-Se ternary system

In the case of the H-C-Se ternary system, the number of structures found in the MHM runs were 236. The compounds from Tables 5.1 and 5.2 used to define the convex hull were the numbers 7, 25, 27, 28, 40, 48, 49 and 52.

As we can see in Table 5.5, all compounds are above the 50 meV/atom limit we imposed, with the lowest one being 100 meV/atom above the hull. For completeness, we will show the three closest compounds to the convex hull, however, these are less likely to be synthesizable than the thermodynamically stable and metastable compounds in the other ternary systems, at least at 150 GPa.

H_7CSe is 100 meV/atom above the convex hull, followed by H_6CSe at 129 meV/atom and by H_7CSe_2 130 meV/atom above the convex hull. The other compounds are between a distance to the convex hull of 130 to 300 meV/atom, therefore they are even less likely to be able to be synthesized at this pressure. The phase diagram can be viewed in Figure 5.7.

We calculated the electronic band structure and DOS of the previously named three materials of Table 5.4, H_7CSe, H_6CSe and H_7CSe_2. The electronic bands structures and DOS in Figures 5.8, 5.9 and 5.10 confirm these are metals.

In addition, the electronic band structures and DOS in Figure 5.9, in spite of having a convex hull energy distance of 130 meV/atom, seem to have a peak at the Fermi energy. This peak suggests a possible superconductor considering that peaks in the DOS around the Fermi level are a common feature for conventional high T_c superconductors [5].

We also present the crystal structures of each of these three materials in Figure 5.11, made with the aid of the VESTA software with a description of the respective crystal structure.

Table 5.5: Summary of results for the H-C-Se ternary system, at 150 GPa, ordered from the lowest to the highest energy distance from the convex hull. The compound; number of atom in the structure (N_{atoms}); energy distance to the convex hull in meV/atom (E_{hull}); space group (spgrp); and Band gap in eV. The compounds from Tables 5.1 and 5.2 used to make the convex hull were the numbers 7, 25, 27, 28, 40, 48, 49 and 52.

Compound	N_{atoms}	E_{hull} [meV/atom]	spgrp	Band gap [eV]
H_7CSe	18	100	2	0.0
H_6CSe	8	129	6	0.0
H_7CSe_2	20	130	1	0.0
H_6CSe_2	9	147	8	0.0
H_7C_2Se	10	148	1	0.0
H_4CSe	12	154	9	0.0
H_4CSe_2	14	172	2	0.0
H_5CSe	14	175	46	0.0
H_6C_2Se	9	182	8	0.0
$H_6C_2Se_2$	10	193	2	0.0
$H_7C_2Se_2$	11	209	1	0.0
H_4C_2Se	7	219	69	0.0
H_3C_2Se	6	243	8	0.0
H_3CSe	10	255	2	0.0
H_3CSe_2	6	271	8	0.0
$H_3C_2Se_2$	7	298	1	0.0

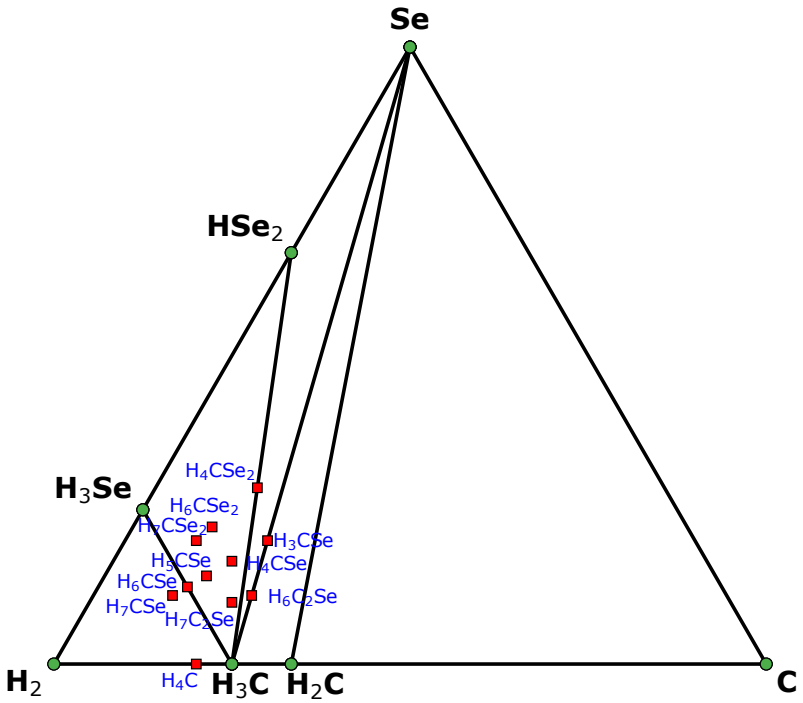

Figure 5.7: Phase diagram of the H-C-Se ternary system at 150 GPa. In green we have the thermodynamically stable compounds and, in red, the compounds above the convex hull.

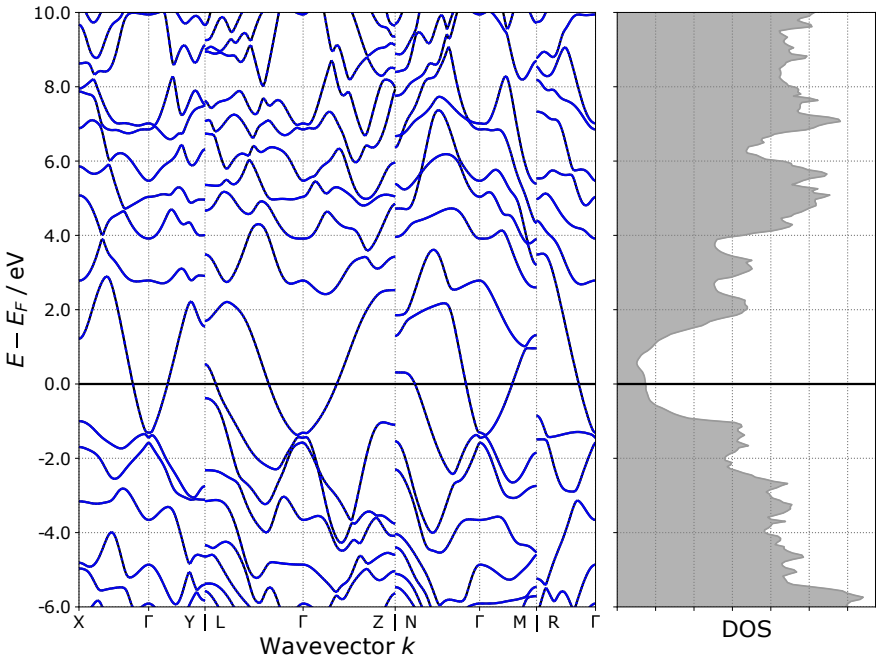

Figure 5.8: Electronic band structure of $P\bar{1}$-H_7CSe with an energy above the convex hull equal to 100 meV/atom. In the vertical axis, we set the Fermi energy at zero. In the horizontal axis, in the electronic band structure we have the high symmetry points; on the right we have the total density of states.

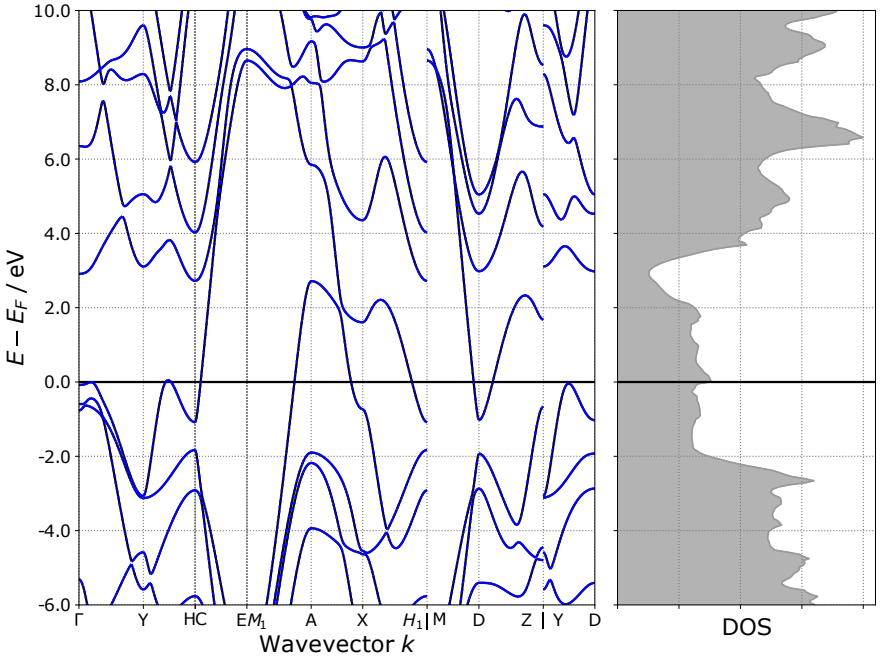

Figure 5.9: Electronic band structure of Pm-H_6CSe with an energy above the convex hull equal to 129 meV/atom. In the vertical axis, we set the Fermi energy at zero. In the horizontal axis, in the electronic band structure we have the high symmetry points; on the right we have the total density of states.

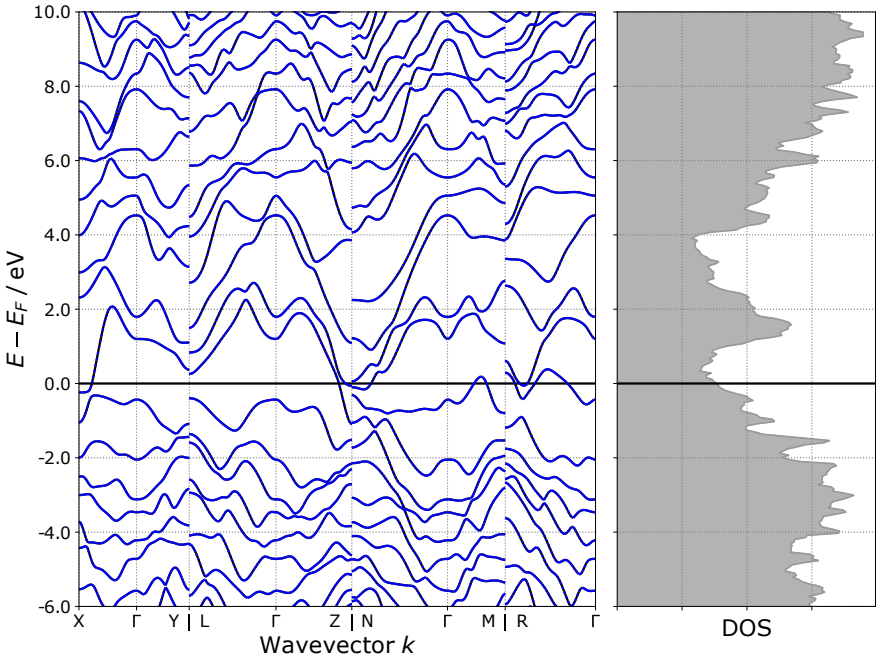

Figure 5.10: Electronic band structure of $P1$-H_7CSe_2 with an energy above the convex hull equal to 130 meV/atom. In the vertical axis, we set the Fermi energy at zero. In the horizontal axis, in the electronic band structure we have the high symmetry points; on the right we have the total density of states.

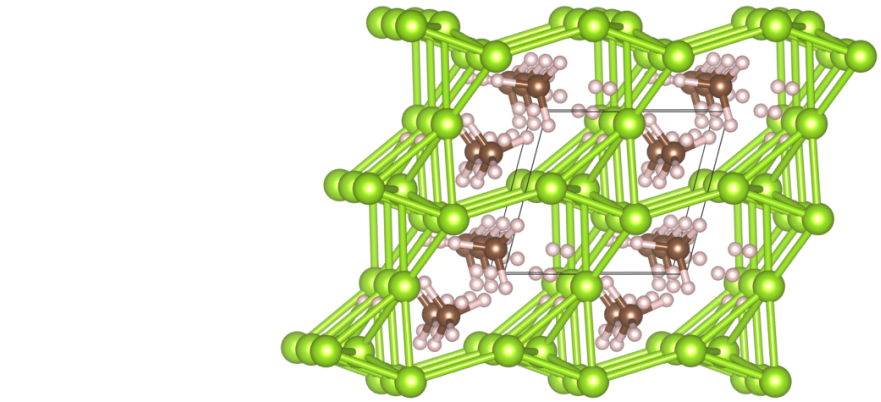

(a) $P1$-H_7CSe_2.

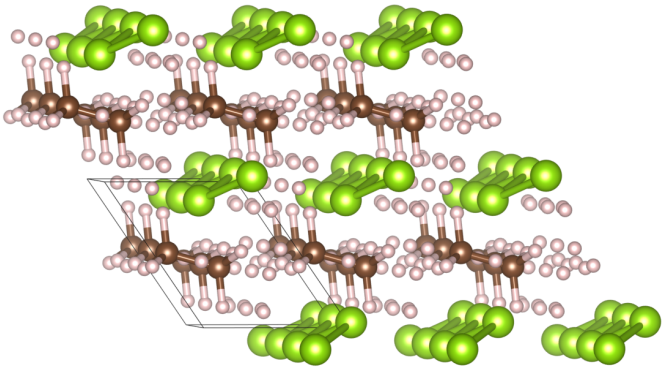

(b) $P\bar{1}$-H_7CSe.

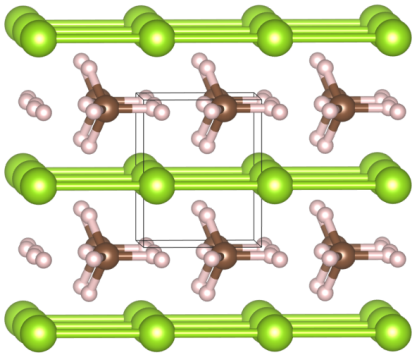

(c) Pm-H_6CSe.

Figure 5.11: Crystal structure of the compounds from the band structures presented from the H-C-Se ternary system. We have hydrogen (H) in pink, carbon (C) in brown and selenium (Se) in light green.

- H_7CSe_2 in Figure 5.11(a) has what could be described as "porous Se structure" with the C and H atoms in between, with what may be some "methane like shape" molecules along with the remaining H atoms.
- H_7CSe in Figure 5.11(b) has threads of zigzagging Se atoms and what may be some "ethane like shape" molecules along with the remaining H atoms.
- H_6CSe in Figure 5.11(c) has what may be some "methane like shape" molecules along with the remaining H atoms. These are surrounding the strait Se atom lines.

5.2.3 Mg-H-Se ternary system

Finally, for the Mg-H-Se ternary system, the number of structures found in the MHM runs were 192. The compounds from Tables 5.1 and 5.2 used to define the convex hull were the numbers 7, 24, 25, 28, 40, 41, 42, 45 and 46.

As we can see in Table 5.6, four compounds: Mg_2H_3Se, MgH_6Se, Mg_2H_6Se and MgH_4Se that are on the convex hull, which mean they are thermodynamically stable. Other four compounds are metastable since they are below 50 meV/atom: MgH_7Se at 17 meV/atom; $Mg_2H_3Se_2$ at 28 meV/atom; MgH_4Se_2 at 36 meV/atom; and MgH_5Se at 46 meV/atom. The remaining ones are between 50 to 120 meV/atom above the convex hull, therefore they are less likely to be able to be synthesized. The phase diagram can be viewed in Figure 5.12.

We calculated the electronic band structure and DOS for the following materials: $Cmm2$- and $P\bar{3}m1$-Mg_2H_3Se, both thermodynamically stable; and $Immm$-MgH_4Se_2, metastable, with 36 meV/atom above hull. These were the two closest metallic compounds to the convex hull plus the forth metallic one of Table 5.4.

The electronic bands structures and DOS of MgH_6Se, Mg_2H_3Se and MgH_4Se_2 in Figures 5.13, 5.14 and 5.15, respectively, confirm these are metals.

We would like to point that $Immm$-MgH_4Se_2, in the band structure and DOS of Figure 5.15, caught our attention because, being within a reasonable distance to the convex hull, 36 meV/atom, seems to have some kind of peak, although flattened[3], at the Fermi energy. This might be good indication for a possible superconductor considering that peaks in the DOS around the Fermi level are a common feature for conventional high T_c superconductors [5]. We will see if this metastable $Immm$-MgH_4Se_2 will unveil superconductivity at the present conditions or at higher pressures.

We also present the crystal structures of $Immm$-MgH_4Se_2, $P\bar{3}m1$-MgH_3Se and $Cmm2$-MgH_6Se in Figure 5.16, made with the aid of the VESTA software with a description of the respective crystal structure.

[3] The sharper the peak, the higher the T_c [5].

Table 5.6: Convex hull data of the Mg-H-Se ternary system, at 150 GPa, ordered from the lowest to the highest energy distance from the convex hull. The compound; number of atom in the structure (N_{atoms}); energy distance to the convex hull in meV/atom (E_{hull}); space group (spgrp); and Band gap in eV. The compounds from Tables 5.1 and 5.2 used to make the convex hull were the numbers 7, 24, 25, 28, 40, 41, 42, 45 and 46.

Compound	N_{atoms}	E_{hull} [meV/atom]	spgrp	Band gap [eV]
Mg_2H_3Se	6	0	164	0.0
MgH_6Se	8	0	35	0.0
Mg_2H_6Se	9	0	38	1.2
MgH_4Se	12	0	8	1.7
MgH_7Se	18	17	8	1.0
$Mg_2H_3Se_2$	7	28	44	0.0
MgH_4Se_2	14	36	71	0.0
MgH_5Se	14	46	8	0.2
$Mg_2H_7Se_2$	22	54	1	1.1
$Mg_2H_6Se_2$	20	59	1	0.6
MgH_3Se	10	59	63	0.0
Mg_2H_4Se	7	63	164	1.4
MgH_6Se_2	9	66	12	0.0
MgH_7Se_2	10	79	1	0.0
Mg_2H_7Se	10	85	166	0.0
MgH_3Se_2	12	115	15	0.0

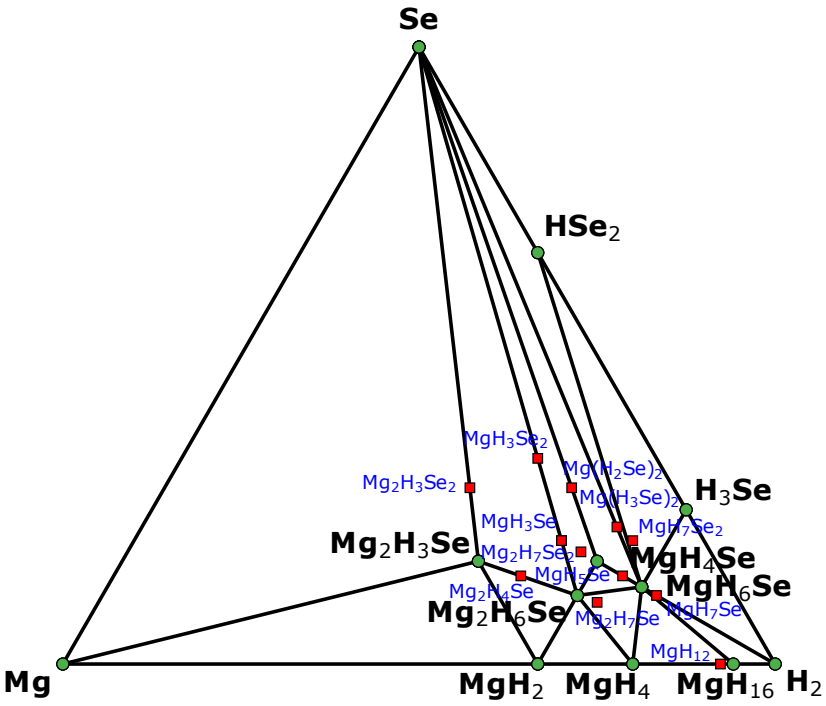

Figure 5.12: Phase diagram of the Mg-H-Se ternary system at 150 GPa. In green we have the thermodynamically stable compounds and, in red, the compounds above the convex hull.

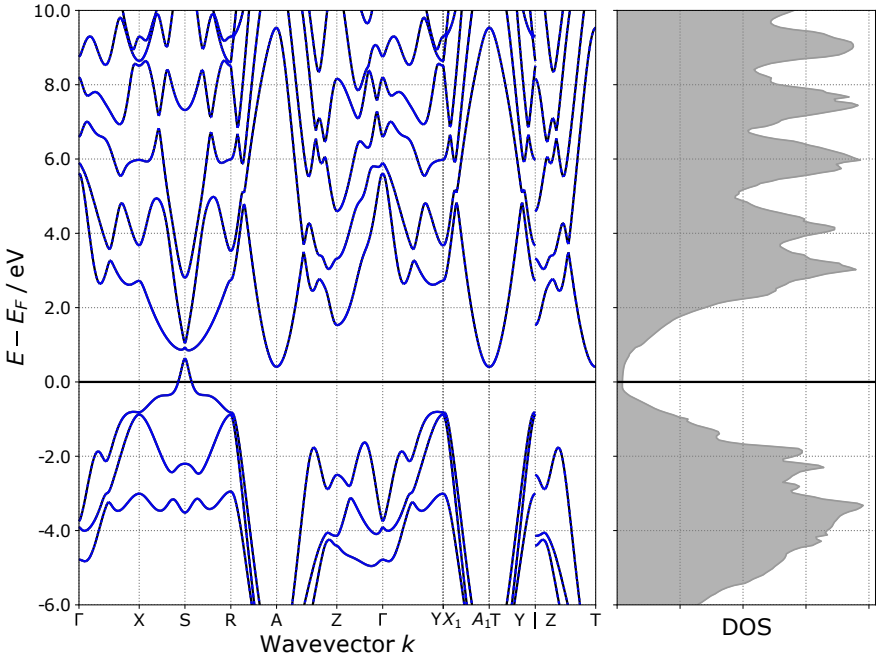

Figure 5.13: Electronic band structure of $Cmm2$-MgH_6Se on the convex hull. In the vertical axis, we set the Fermi energy at zero. In the horizontal axis, in the electronic band structure we have the high symmetry points; on the right we have the total density of states.

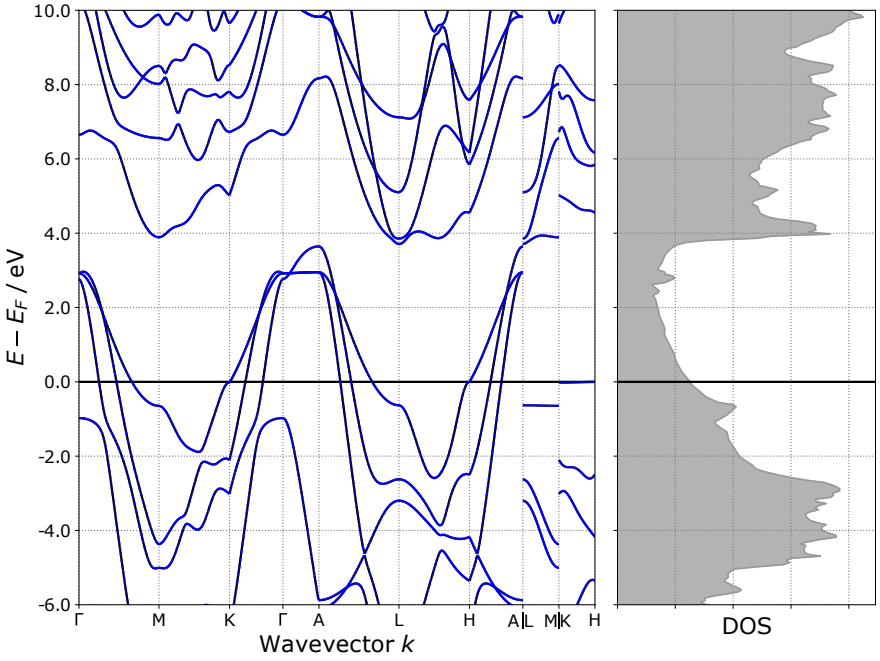

Figure 5.14: Electronic band structure of $P\bar{3}m1$-Mg_2H_3Se on the convex hull. In the vertical axis, we set the Fermi energy at zero. In the horizontal axis, in the electronic band structure we have the high symmetry points; on the right we have the total density of states.

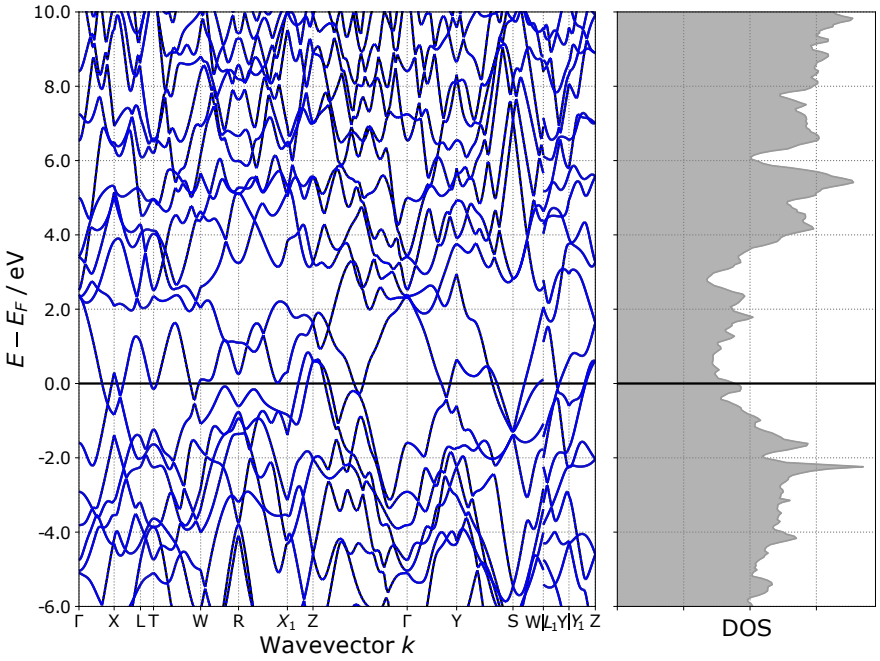

Figure 5.15: Electronic band structure of $Immm$-MgH_4Se_2 with an energy above the convex hull equal to 36 meV/atom. In the vertical axis, we set the Fermi energy at zero. In the horizontal axis, in the electronic band structure we have the high symmetry points; on the right we have the total density of states.

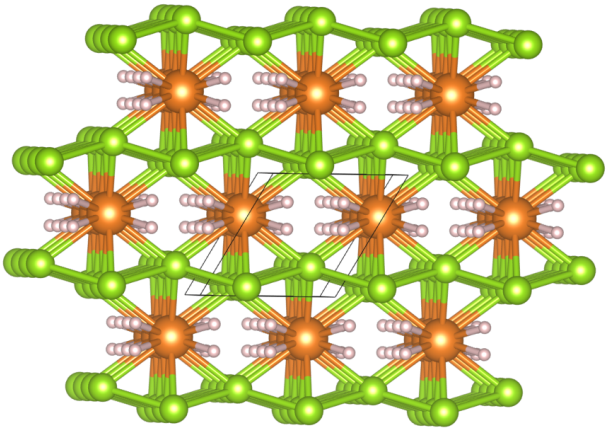

(a) $Immm$-MgH_4Se_2

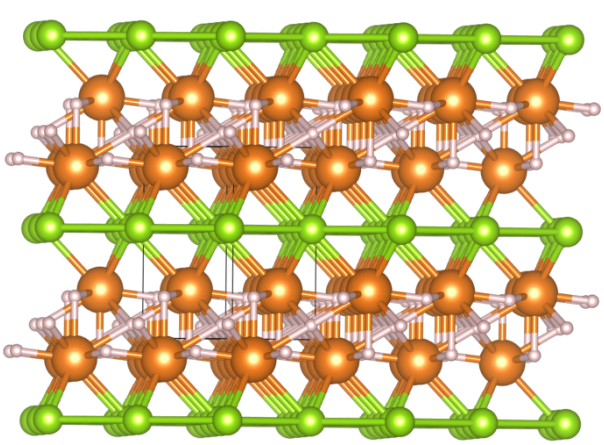

(b) $P\bar{3}m1$-Mg_2H_3Se.

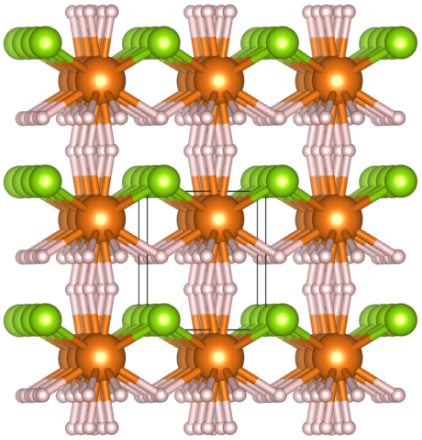

(c) $Cmm2$-MgH_6Se.

Figure 5.16: Crystal structure of the compounds from the band structures presented from the Mg-H-Se ternary system. We have magnesium (Mg) in orange, hydrogen (H) in a pink and selenium (Se) in light green.

- MgH_4Se_2 in Figure 5.16(a) has Mg atoms almost circled by H atoms. This is separated by a zigzag layer of Se atoms that is made of interconnected triangular structure.
- Mg_2H_3Se in Figure 5.16(b) has H atoms concentrated around and in between the two planes of Mg atoms that are arrange in triangular shapes which, if view from the top, will have a honeycomb shape. This is separated by layers of Se atoms, similar to the structure in Figure 5.16(a) but in a strait plane.
- MgH_6Se in Figure 5.16(c) has each of the Mg and Se atoms in the vertices of their own cobblestone shape, with an offset. The H atoms, compared to the Se atoms, stay in the opposite side of the Mg plane and at the top an bottom of each Mg atom.

Chapter 6

Conclusions and future work

In summary, with the ambition of finding thermdynamically stable metallic compounds in the selected systems, Li-C-S, H-C-Se and Mg-H-Se, at a pressure of 150 GPa, we applied the MHM algorithm to search the PES of each system.

On the one hand, the lowest energy distance to the convex hull in the H-C-Se ternary system was 100 meV/atom, $P\bar{1}$-H_7CSe. On the other hand, in the two ternary systems, Li-C-S and Mg-H-Se, we successfully found five metallic compounds within the 50 meV/atom energy distance to the convex hull. From those, two are thermodynamically stable compounds. These five compounds are: $P\bar{3}m1$-Mg_2H_3Se and $Cmm2$-MgH_6Se, both thermodynamically stable, and $Imm2$-$Mg_2H_3Se_2$, $Immm$$MgH_4Se_2$ and $P\bar{1}$-Li_6CS with a energy distance to the convex hull of 28 meV/atom, 36 meV/atom and 28 meV/atom, respectively.

High pressure search for new stable compounds, above 150 GPa, in the Mg-H-Se ternary system seems promising compared to the Li-C-S and H-C-Se ternary systems. Not only did we obtain the most stable and metastable compounds from the Mg-H-Se ternary system but also the remaining compounds above 50 meV/atom are within 120meV/atom distance to the convex hull which is much less than what we found in the other ternary systems we searched.

Looking at the Li-C-S ternary, we did find 2 compounds within the 50 meV/atom distance to the convex hull although the remaining 13 compounds are between 100 to 500 meV/atom. Unfortunatly, our search results in the H-C-Se ternary system weren't as rewarding as the other systems, nevertheless, the compounds are mainly between 100 to 200 meV/atom, which might actually get better results at higher pressures than the Li-C-S ternary system.

Further studies of these search results will continue in our future work.

Future work involves the dynamic stability assessment through phonon spectrum calculations

and calculations to find the critical temperature of a possible superconductor. Subsequently, depending on the outcome of the work ahead, we will proceed to higher pressure searches.

Despite the fact that the work does not end here, it is a encouraging start.

The POSCAR[1] files of the structures in the phase diagrams in Figures 5.2, 5.7 and 5.12 will be made available in the GitLab repository [79].

[1]Files with the structure information used by VASP.

References

[1] E. Snider, N. Dasenbrock-Gammon, R. McBride, M. Debessai, H. Vindana, K. Vencatasamy, K. V. Lawler, A. Salamat, and R. P. Dias, "Room-temperature superconductivity in a carbonaceous sulfur hydride," , vol. 586, no. 7829, pp. 373–377, Oct. 2020. [Online]. Available: https://ui.adsabs.harvard.edu/abs/2020Natur.586..373S

[2] N. W. Ashcroft, "Metallic hydrogen: A high-temperature superconductor?" *Phys. Rev. Lett.*, vol. 21, pp. 1748–1749, Dec 1968. [Online]. Available: https://link.aps.org/doi/10.1103/PhysRevLett.21.1748

[3] ——, "Hydrogen dominant metallic alloys: High temperature superconductors?" *Phys. Rev. Lett.*, vol. 92, p. 187002, May 2004. [Online]. Available: https://link.aps.org/doi/10.1103/PhysRevLett.92.187002

[4] J. A. Flores-Livas, L. Boeri, A. Sanna, G. Profeta, R. Arita, and M. Eremets, "A perspective on conventional high-temperature superconductors at high pressure: Methods and materials," *Physics Reports*, vol. 856, pp. 1–78, 2020, a perspective on conventional high-temperature superconductors at high pressure: Methods and materials. [Online]. Available: https://www.sciencedirect.com/science/article/pii/S0370157320300363

[5] M. Gubler, J. A. Flores-Livas, A. Kozhevnikov, and S. Goedecker, "Missing theoretical evidence for conventional room-temperature superconductivity in low-enthalpy structures of carbonaceous sulfur hydrides," *Phys. Rev. Materials*, vol. 6, p. 014801, Jan 2022. [Online]. Available: https://link.aps.org/doi/10.1103/PhysRevMaterials.6.014801

[6] J. E. Hirsch and F. Marsiglio, "Unusual width of the superconducting transition in a hydride," *Nature*, vol. 596, no. 7873, pp. E9–E10, aug 2021. [Online]. Available: https://doi.org/10.1038%2Fs41586-021-03595-z

[7] M. Dogan and M. L. Cohen, "Anomalous behavior in high-pressure carbonaceous sulfur hydride," *Physica C: Superconductivity and its Applications*, vol. 583, p. 1353851, 2021. [Online]. Available: https://www.sciencedirect.com/science/article/pii/S0921453421000344

[8] J. E. Hirsch, "Faulty evidence for superconductivity in ac magnetic susceptibility of sulfur hydride under pressure," 2021. [Online]. Available: https://arxiv.org/abs/2109.08517

[9] B. Li, C. Ji, W. Yang, J. Wang, K. Yang, R. Xu, W. Liu, Z. Cai, J. Chen, and H. kwang Mao, "Diamond anvil cell behavior up to 4 mbar," *Proceedings of the National Academy of Sciences*, vol. 115, no. 8, pp. 1713–1717, 2018. [Online]. Available: https://www.pnas.org/doi/abs/10.1073/pnas.1721425115

[10] L. Dubrovinsky, N. Dubrovinskaia, E. Bykova, M. Bykov, V. Prakapenka, C. Prescher, K. Glazyrin, H.-P. Liermann, M. Hanfland, M. Ekholm, Q. Feng, L. V. Pourovskii, M. I. Katsnelson, J. M. Wills, and I. A. Abrikosov, "The most incompressible metal osmium at static pressures above 750 gigapascals," *Nature*, vol. 525, no. 7568, pp. 226–229, Sep 2015. [Online]. Available: https://doi.org/10.1038/nature14681

[11] Wikipedia, "Diamond anvil cell — Wikipedia, the free encyclopedia," http://en.wikipedia.org/w/index.php?title=Diamond%20anvil%20cell&oldid=1107219380, 2022, [Online; accessed 13-September-2022].

[12] T. Bi, A. Shamp, T. Terpstra, R. J. Hemley, and E. Zurek, "The Li–F–H ternary system at high pressures," *The Journal of Chemical Physics*, vol. 154, no. 12, p. 124709, Mar 2021. [Online]. Available: http://dx.doi.org/10.1063/5.0041490

[13] S. Zhang, Q. Yang, X. Zhang, K. Zhao, H. Yu, L. Zhu, and H. Liu, "Crystal structures and superconductivity of lithium and fluorine implanted gold hydrides under high pressures," *Phys. Chem. Chem. Phys.*, vol. 23, pp. 21 544–21 553, 2021. [Online]. Available: http://dx.doi.org/10.1039/D1CP02781F

[14] J. Zheng, W. Sun, X. Dou, A.-J. Mao, and C. Lu, "Pressure-driven structural phase transitions and superconductivity of ternary hydride $MgVH_6$," *The Journal of Physical Chemistry C*, vol. 125, no. 5, pp. 3150–3156, 2021. [Online]. Available: https://doi.org/10.1021/acs.jpcc.0c09447

[15] J. Chen, X. Xue, H. Chen, H. Liu, Q. Zang, and W. Lu, "Theoretical study on Fe–Se–H hydrides under high pressure," *The Journal of Physical Chemistry C*, vol. 123, no. 46, pp. 28 008–28 014, 2019. [Online]. Available: https://doi.org/10.1021/acs.jpcc.9b06504

[16] X. Liang, S. Zhao, C. Shao, A. Bergara, H. Liu, L. Wang, R. Sun, Y. Zhang, Y. Gao, Z. Zhao, X.-F. Zhou, J. He, D. Yu, G. Gao, and Y. Tian, "First-principles study of crystal structures and superconductivity of ternary YSH_6 and $LaSH_6$ at high pressures," *Phys. Rev. B*, vol. 100, p. 184502, Nov 2019. [Online]. Available: https://link.aps.org/doi/10.1103/PhysRevB.100.184502

[17] P. Song, Z. Hou, P. Baptista de Castro, K. Nakano, K. Hongo, Y. Takano, and R. Maezono, "High-pressure Mg–Sc–H phase diagram and its superconductivity from first-principles calculations," *The Journal of Physical Chemistry C*, Jan 2022. [Online]. Available: http://dx.doi.org/10.1021/acs.jpcc.1c08743

[18] Y. K. Wei, L. Q. Jia, Y. Y. Fang, L. J. Wang, Z. X. Qian, J. N. Yuan, G. Selvaraj, G. F. Ji, and D. Q. Wei, "Formation and superconducting properties of predicted ternary hydride $ScYH_6$ under pressures," *International Journal of Quantum Chemistry*, vol. 121, no. 4, p. e26459. [Online]. Available: https://onlinelibrary.wiley.com/doi/abs/10.1002/qua.26459

[19] P. Zhang, Y. Sun, X. Li, J. Lv, and H. Liu, "Structure and superconductivity in compressed Li-Si-H compounds: Density functional theory calculations," *Phys. Rev. B*, vol. 102, p. 184103, Nov 2020. [Online]. Available: https://link.aps.org/doi/10.1103/PhysRevB.102.184103

[20] H. Song, Z. Zhang, M. Du, Q. Jiang, D. Duan, and T. Cui, "Phase diagrams and superconductivity of ternary na-al-h compounds at high pressure," *Phys. Rev. B*, vol. 104, p. 104509, Sep 2021. [Online]. Available: https://link.aps.org/doi/10.1103/PhysRevB.104.104509

[21] Y. Ma, D. Duan, Z. Shao, H. Yu, H. Liu, F. Tian, X. Huang, D. Li, B. Liu, and T. Cui, "Divergent synthesis routes and superconductivity of ternary hydride $MgSiH_6$ at high pressure," *Phys. Rev. B*, vol. 96, p. 144518, Oct 2017. [Online]. Available: https://link.aps.org/doi/10.1103/PhysRevB.96.144518

[22] Y. Ma, D. Duan, Z. Shao, D. Li, L. Wang, H. Yu, F. Tian, H. Xie, B. Liu, and T. Cui, "Prediction of superconducting ternary hydride $MgGeH_6$: from divergent high-pressure formation routes," *Phys. Chem. Chem. Phys.*, vol. 19, pp. 27 406–27 412, 2017. [Online]. Available: http://dx.doi.org/10.1039/C7CP05267G

[23] B. Li, W. Yang, H. Chen, L. Zhao, L. Chen, K. Yang, and W. Lu, "Study on superconducting Li–Se–H hydrides," *Phys. Chem. Chem. Phys.*, vol. 24, pp. 8415–8421, 2022. [Online]. Available: http://dx.doi.org/10.1039/D1CP04963A

[24] S. Di Cataldo, W. von der Linden, and L. Boeri, "Phase diagram and superconductivity of calcium borohyrides at extreme pressures," *Phys. Rev. B*, vol. 102, p. 014516, Jul 2020. [Online]. Available: https://link.aps.org/doi/10.1103/PhysRevB.102.014516

[25] H. Liu, R. Cheng, K. Yang, B. Li, L. Chen, and W. Lu, "Theoretical study on the Y-Ba-H hydrides at high pressure," *Physics Letters A*, vol. 390, p. 127109, 2021. [Online]. Available: https://www.sciencedirect.com/science/article/pii/S0375960120309762

[26] X. Liang, A. Bergara, X. Wei, X. Song, L. Wang, R. Sun, H. Liu, R. J. Hemley, L. Wang, G. Gao, and Y. Tian, "Prediction of high-tc superconductivity in ternary lanthanum borohydrides," *Physical Review B*, vol. 104, no. 13, Oct 2021. [Online]. Available: http://dx.doi.org/10.1103/PhysRevB.104.134501

[27] Y. Yan, T. Bi, N. Geng, X. Wang, and E. Zurek, "A metastable $CaSH_3$ phase composed of hs honeycomb sheets that is superconducting under pressure," *The Journal of Physical Chemistry Letters*, vol. 11, no. 22, pp. 9629–9636, 2020, pMID: 33125247. [Online]. Available: https://doi.org/10.1021/acs.jpclett.0c02299

[28] C. Kokail, W. von der Linden, and L. Boeri, "Prediction of high-T_c conventional superconductivity in the ternary lithium borohydride system," *Phys. Rev. Materials*, vol. 1, p. 074803, Dec 2017. [Online]. Available: https://link.aps.org/doi/10.1103/PhysRevMaterials.1.074803

[29] Y. Liu, Y. Sun, and P. Gao, "The superconductivity of N–Si–H compounds at high pressure," *Solid State Communications*, vol. 329, p. 114260, 2021. [Online]. Available: https://www.sciencedirect.com/science/article/pii/S0038109821000715

[30] S. Di Cataldo, C. Heil, W. von der Linden, and L. Boeri, "$LaBH_8$: Towards high-T_c low-pressure superconductivity in ternary superhydrides," *Phys. Rev. B*, vol. 104, p. L020511, Jul 2021. [Online]. Available: https://link.aps.org/doi/10.1103/PhysRevB.104.L020511

[31] L. Chen, X. Xue, H. Chen, B. Li, K. Yang, and W. Lu, "Superconductivity of K-Y-H hydrides under high pressure," *Physics Letters A*, vol. 420, p. 127750, 2021. [Online]. Available: https://www.sciencedirect.com/science/article/pii/S0375960121006149

[32] Z. Shao, D. Duan, Y. Ma, H. Yu, H. Song, H. Xie, D. Li, F. Tian, B. Liu, T. Cui, and et al., "Ternary superconducting cophosphorus hydrides stabilized via lithium," *Nature News*, Oct 2019. [Online]. Available: https://www.nature.com/articles/s41524-019-0244-6

[33] H. Xie, D. Duan, Z. Shao, H. Song, Y. Wang, X. Xiao, F. Tian, B. Liu, and T. Cui, "High-temperature superconductivity in ternary clathrate $YCaH_{12}$ under high pressures," *Journal of Physics: Condensed Matter*, vol. 31, 02 2019. [Online]. Available: http://dx.doi.org/10.1088/1361-648X/ab09b4

[34] X. Liang, A. Bergara, L. Wang, B. Wen, Z. Zhao, X.-F. Zhou, J. He, G. Gao, and Y. Tian, "Potential high-T_c superconductivity in $CaYH_{12}$ under pressure," *Phys. Rev. B*, vol. 99, p. 100505, Mar 2019. [Online]. Available: https://link.aps.org/doi/10.1103/PhysRevB.99.100505

[35] W. Sukmas, P. Tsuppayakorn-aek, U. Pinsook, and T. Bovornratanaraks, "Near-room-temperature superconductivity of Mg/Ca substituted metal hexahydride under pressure," *Journal of Alloys and Compounds*, vol. 849, p. 156434, 2020. [Online]. Available: https://www.sciencedirect.com/science/article/pii/S0925838820327985

[36] Y. Sun, J. Lv, Y. Xie, H. Liu, and Y. Ma, "Route to a superconducting phase above room temperature in electron-doped hydride compounds under high pressure," *Phys. Rev. Lett.*, vol. 123, p. 097001, Aug 2019. [Online]. Available: https://link.aps.org/doi/10.1103/PhysRevLett.123.097001

[37] A. M. Shipley, M. J. Hutcheon, R. J. Needs, and C. J. Pickard, "High-throughput discovery of high-temperature conventional superconductors," *Physical Review B*, vol. 104, no. 5, Aug 2021. [Online]. Available: http://dx.doi.org/10.1103/PhysRevB.104.054501

[38] G. Kresse and J. Furthmüller, "Efficiency of ab-initio total energy calculations for metals and semiconductors using a plane-wave basis set," *Computational*

Materials Science, vol. 6, no. 1, pp. 15–50, 1996. [Online]. Available: https://www.sciencedirect.com/science/article/pii/0927025696000080

[39] G. Kresse and J. Furthmüller, "Efficient iterative schemes for ab initio total-energy calculations using a plane-wave basis set," *Phys. Rev. B*, vol. 54, pp. 11 169–11 186, Oct 1996. [Online]. Available: https://link.aps.org/doi/10.1103/PhysRevB.54.11169

[40] G. Kresse and D. Joubert, "From ultrasoft pseudopotentials to the projector augmented-wave method," *Phys. Rev. B*, vol. 59, pp. 1758–1775, Jan 1999. [Online]. Available: https://link.aps.org/doi/10.1103/PhysRevB.59.1758

[41] P. Giannozzi, S. Baroni, N. Bonini, M. Calandra, R. Car, C. Cavazzoni, D. Ceresoli, G. L. Chiarotti, M. Cococcioni, I. Dabo, A. D. Corso, S. de Gironcoli, S. Fabris, G. Fratesi, R. Gebauer, U. Gerstmann, C. Gougoussis, A. Kokalj, M. Lazzeri, L. Martin-Samos, N. Marzari, F. Mauri, R. Mazzarello, S. Paolini, A. Pasquarello, L. Paulatto, C. Sbraccia, S. Scandolo, G. Sclauzero, A. P. Seitsonen, A. Smogunov, P. Umari, and R. M. Wentzcovitch, "QUANTUM ESPRESSO: a modular and open-source software project for quantum simulations of materials," *Journal of Physics: Condensed Matter*, vol. 21, no. 39, p. 395502, sep 2009. [Online]. Available: https://doi.org/10.1088/0953-8984/21/39/395502

[42] P. Giannozzi, O. Andreussi, T. Brumme, O. Bunau, M. B. Nardelli, M. Calandra, R. Car, C. Cavazzoni, D. Ceresoli, M. Cococcioni, N. Colonna, I. Carnimeo, A. D. Corso, S. de Gironcoli, P. Delugas, R. A. DiStasio, A. Ferretti, A. Floris, G. Fratesi, G. Fugallo, R. Gebauer, U. Gerstmann, F. Giustino, T. Gorni, J. Jia, M. Kawamura, H.-Y. Ko, A. Kokalj, E. Küçükbenli, M. Lazzeri, M. Marsili, N. Marzari, F. Mauri, N. L. Nguyen, H.-V. Nguyen, A. O. de-la Roza, L. Paulatto, S. Poncé, D. Rocca, R. Sabatini, B. Santra, M. Schlipf, A. P. Seitsonen, A. Smogunov, I. Timrov, T. Thonhauser, P. Umari, N. Vast, X. Wu, and S. Baroni, "Advanced capabilities for materials modelling with quantum ESPRESSO," *Journal of Physics: Condensed Matter*, vol. 29, no. 46, p. 465901, oct 2017. [Online]. Available: https://doi.org/10.1088%2F1361-648x%2Faa8f79

[43] S. J. Clark, M. D. Segall, C. J. Pickard, P. J. Hasnip, M. I. J. Probert, K. Refson, and M. C. Payne, "First principles methods using castep," *Zeitschrift für Kristallographie - Crystalline Materials*, vol. 220, no. 5-6, pp. 567–570, 2005. [Online]. Available: https://doi.org/10.1524/zkri.220.5.567.65075

[44] A. R. Oganov, *Modern methods of crystal structure prediction.* John Wiley & Sons, 2011.

[45] M. Amsler and S. Goedecker, "Crystal structure prediction using the minima hopping method," *The Journal of Chemical Physics*, vol. 133, no. 22, p. 224104, 2010. [Online]. Available: https://doi.org/10.1063/1.3512900

[46] S. Goedecker, "Minima hopping: An efficient search method for the global minimum of the potential energy surface of complex molecular systems," *The Journal of Chemical Physics*, vol. 120, no. 21, pp. 9911–9917, 2004. [Online]. Available: https://doi.org/10.1063/1.1724816

[47] C. Fiolhais, F. Nogueira, and M. Marques, *A primer in density functional.* Springer, 2011.

[48] A. Szabo and N. S. Ostlund, *Modern Quantum Chemistry: Introduction to Advanced Electronic Structure Theory.* McGraw-Hill, 1996.

[49] W. Koch and M. C. Holthausen, *A chemist's guide to density functional theory.* Wiley-VCH, 2010.

[50] P. Hohenberg and W. Kohn, "Inhomogeneous electron gas," *Phys. Rev.*, vol. 136, pp. B864–B871, Nov 1964. [Online]. Available: https://link.aps.org/doi/10.1103/PhysRev.136.B864

[51] F. Nogueira, "Descrição de propriedades físicas de sólidos e agregados com pseudopotenciais," Ph.D. dissertation, Faculty of Sciences and Technology, University of Coimbra, 1999.

[52] F. Giustino, *Materials modelling using density functional theory: Properties and predictions.* Oxford University Press, 2014.

[53] R. G. Parr and W. Yang, *Density-functional theory of atoms and molecules.* Oxford University Press, 1994.

[54] R. M. Martin, *Electronic structure: Basic theory and practical methods.* Cambridge University Press, 2008.

[55] W. Kohn and L. J. Sham, "Self-consistent equations including exchange and correlation effects," *Phys. Rev.*, vol. 140, pp. A1133–A1138, Nov 1965. [Online]. Available: https://link.aps.org/doi/10.1103/PhysRev.140.A1133

[56] A. Gavezzotti, "Are crystal structures predictable?" *Accounts of Chemical Research*, vol. 27, no. 10, pp. 309–314, 1994. [Online]. Available: https://doi.org/10.1021/ar00046a004

[57] S. E. Schönborn, S. Goedecker, S. Roy, and A. R. Oganov, "The performance of minima hopping and evolutionary algorithms for cluster structure prediction," *The Journal of Chemical Physics*, vol. 130, no. 14, p. 144108, 2009. [Online]. Available: https://doi.org/10.1063/1.3097197

[58] S. Roy, S. Goedecker, and V. Hellmann, "Bell-evans-polanyi principle for molecular dynamics trajectories and its implications for global optimization," *Phys. Rev. E*, vol. 77, p. 056707, May 2008. [Online]. Available: https://link.aps.org/doi/10.1103/PhysRevE.77.056707

[59] J. A. Flores-Livas, M. Amsler, T. J. Lenosky, L. Lehtovaara, S. Botti, M. A. L. Marques, and S. Goedecker, "High-pressure structures of disilane and their superconducting properties," *Phys. Rev. Lett.*, vol. 108, p. 117004, Mar 2012. [Online]. Available: https://link.aps.org/doi/10.1103/PhysRevLett.108.117004

[60] T. F. Cerqueira, "Structural prediction and materials design," Ph.D. dissertation, Faculty of Physics and Astronomy, Friedrich-Schiller University, Jena, 2016.

[61] Y. Hinuma, T. Hatakeyama, Y. Kumagai, L. A. Burton, H. Sato, Y. Muraba, S. Iimura, H. Hiramatsu, I. Tanaka, H. Hosono, and F. Oba, "Discovery of earth-abundant nitride semiconductors by computational screening and high-pressure synthesis," *Nature Communications*, vol. 7, no. 1, p. 11962, Jun 2016. [Online]. Available: https://doi.org/10.1038/ncomms11962

[62] T. Bi, A. Shamp, T. Terpstra, R. J. Hemley, and E. Zurek, "The li–f–h ternary system at high pressures," *The Journal of Chemical Physics*, vol. 154, no. 12, p. 124709, 2021. [Online]. Available: https://doi.org/10.1063/5.0041490

[63] B. Li, W. Yang, H. Chen, L. Zhao, L. Chen, K. Yang, and W. Lu, "Study on superconducting Li–Se–H hydrides," *Phys. Chem. Chem. Phys.*, vol. 24, pp. 8415–8421, 2022. [Online]. Available: http://dx.doi.org/10.1039/D1CP04963A

[64] P. Borlido, "New first-principles approaches for the structural and electronic properties of two-dimensional materials," Ph.D. dissertation, Faculty of Physics and Astronomy, Friedrich-Schiller University, Jena, 2019.

[65] D. V. Schroeder, *An Introduction to Thermal Physics.* Addison Wesley Longman, 1999.

[66] J. P. Perdew, K. Burke, and M. Ernzerhof, "Generalized gradient approximation made simple," *Phys. Rev. Lett.*, vol. 77, pp. 3865–3868, Oct 1996. [Online]. Available: https://link.aps.org/doi/10.1103/PhysRevLett.77.3865

[67] P. E. Blöchl, "Projector augmented-wave method," *Phys. Rev. B*, vol. 50, pp. 17 953–17 979, Dec 1994. [Online]. Available: https://link.aps.org/doi/10.1103/PhysRevB.50.17953

[68] A. Jain, S. P. Ong, G. Hautier, W. Chen, W. D. Richards, S. Dacek, S. Cholia, D. Gunter, D. Skinner, G. Ceder, and K. A. Persson, "Commentary: The materials project: A materials genome approach to accelerating materials innovation," *APL Materials*, vol. 1, no. 1, p. 011002, 2013. [Online]. Available: https://doi.org/10.1063/1.4812323

[69] S. P. Ong, W. D. Richards, A. Jain, G. Hautier, M. Kocher, S. Cholia, D. Gunter, V. L. Chevrier, K. A. Persson, and G. Ceder, "Python materials genomics (pymatgen): A robust, open-source python library for materials analysis," *Computational Materials Science*, vol. 68, pp. 314–319, 2013. [Online]. Available: https://www.sciencedirect.com/science/article/pii/S0927025612006295

[70] Y. Wu, P. Lazic, G. Hautier, K. Persson, and G. Ceder, "First principles high throughput screening of oxynitrides for water-splitting photocatalysts," *Energy Environ. Sci.*, vol. 6, pp. 157–168, 2013. [Online]. Available: http://dx.doi.org/10.1039/C2EE23482C

[71] K. Momma and F. Izumi, "*VESTA3* for three-dimensional visualization of crystal, volumetric and morphology data," *Journal of Applied Crystallography*, vol. 44, no. 6, pp. 1272–1276, Dec 2011.

[72] C. J. Pickard and R. J. Needs, "Structure of phase iii of solid hydrogen," *Nature Physics*, vol. 3, no. 7, pp. 473–476, Jul 2007. [Online]. Available: https://doi.org/10.1038/nphys625

[73] J. Lv, Y. Wang, L. Zhu, and Y. Ma, "Predicted novel high-pressure phases of lithium," *Phys. Rev. Lett.*, vol. 106, p. 015503, Jan 2011. [Online]. Available: https://link.aps.org/doi/10.1103/PhysRevLett.106.015503

[74] S. Zhang, Y. Wang, J. Zhang, H. Liu, X. Zhong, H.-F. Song, G. Yang, L. Zhang, and Y. Ma, "Phase diagram and high-temperature superconductivity of compressed selenium hydrides," *Scientific Reports*, vol. 5, no. 1, p. 15433, Oct 2015. [Online]. Available: https://doi.org/10.1038/srep15433

[75] D. C. Lonie, J. Hooper, B. Altintas, and E. Zurek, "Metallization of magnesium polyhydrides under pressure," *Phys. Rev. B*, vol. 87, p. 054107, Feb 2013. [Online]. Available: https://link.aps.org/doi/10.1103/PhysRevB.87.054107

[76] H. Liu, I. I. Naumov, and R. J. Hemley, "Dense hydrocarbon structures at megabar pressures," *The Journal of Physical Chemistry Letters*, vol. 7, no. 20, pp. 4218–4222, 2016. [Online]. Available: Https://doi.org/10.1021/acs.jpclett.6b02001

[77] I. Efthimiopoulos, D. E. Benson, S. Konar, J. Nylén, G. Svensson, U. Häussermann, S. Liebig, U. Ruschewitz, G. V. Vazhenin, I. Loa, M. Hanfland, and K. Syassen, "Structural transformations of li_2c_2 at high pressures," *Phys. Rev. B*, vol. 92, p. 064111, Aug 2015. [Online]. Available: https://link.aps.org/doi/10.1103/PhysRevB.92.064111

[78] A. Grzechnik, A. Vegas, K. Syassen, I. Loa, M. Hanfland, and M. Jansen, "Reversible antifluorite to anticotunnite phase transition in Li2S at high pressures," *Journal of Solid State Chemistry*, vol. 154, no. 2, pp. 603–611, 2000. [Online]. Available: https://www.sciencedirect.com/science/article/pii/S0022459600989023

[79] "LiCS HCSe MgHSe Ternary Systems at 150GPa," https://gitlab.com/Joaoqoliveira/LiCS_HCSe_MgHSe_150GPa.

List of Figures

List of Tables